A Theory for the Vertical Alignment of a Quasigeostrophic Vortex

DAVID A. SCHECTER

Advanced Study Program, National Center for Atmospheric Research, Boulder, Colorado*

MICHAEL T. MONTGOMERY AND PAUL D. REASOR+

Department of Atmospheric Science, Colorado State University, Fort Collins, Colorado

(Manuscript received 22 December 2000, in final form 26 June 2001)

ABSTRACT

This article presents a new theory for the rate at which a quasigeostrophic vortex realigns, under conservative dynamics, after being tilted by an episode of external vertical shear. The initial tilt is viewed as the excitation of a three-dimensional ''vortex Rossby mode.'' This mode, that is, the tilt, decays exponentially with time during its early evolution. The decay rate γ is proportional to the potential vorticity gradient at a critical radius, where the fluid rotation is resonant with the mode. The decay rate γ also depends on the internal Rossby deformation radius l_R, which is proportional to the stratification strength of the atmospheric or oceanic layer containing the vortex. The change of γ with l_R is sensitive to the form of the vortex. For the case of a ''Rankine-with-skirt'' vortex, the magnitude of γ increases (initially) with increasing l_R. On the other hand, for the case of a ''Gaussian'' vortex, the magnitude of γ decreases with increasing l_R. The relevance of this theory to tropical cyclogenesis is discussed.

1. Introduction

During its development, an atmospheric or oceanic vortex may experience episodes of external vertical shear. This shear can destroy the vortex before it fully matures. However, many vortices survive, because they have a dominant tendency to stand upright. In this article, we will present a new theory for what drives a vortex to a state of vertical alignment.

Past studies of vertical alignment (Polvani 1991; Viera 1995; Sutyrin et al. 1998; Reasor and Montgomery 2001) typically assume that the Rossby number is much less than unity, so that the dynamics is quasigeostrophic. For simplicity, we will also use the quasigeostrophic approximation. Furthermore, we will neglect diabatic and frictional processes. These effects can be added later.

Figure 1 shows a numerical simulation of the vertical alignment of a quasigeostrophic vortex under conservative dynamics, taken directly from Reasor and Montgomery (2001). The shaded object is an isosurface of potential vorticity (PV). The PV distribution extends radially far beyond this surface. At $t = 0$, the vortex is tilted by an episode of external vertical shear, and then the shear is turned off. In time, the orientation of the tilt rotates, while the amplitude of the tilt decays. Eventually the vortex relaxes to an upright position. We will show that this vertical alignment occurs by the resonant damping of a mode.

The core of a quasigeostrophic vortex can have discrete modes of oscillation (vortex Rossby modes). A misalignment, such as the tilt in Fig. 1, corresponds to the excitation of a discrete core mode. The angular phase velocity of this mode is resonant with the fluid rotation frequency at a critical radius r_* in the outer skirt of the vortex. We will explain how this resonance damps the core mode exponentially with time, provided that the radial derivative of PV at r_* is negative. An analytical expression for the decay rate will be derived and then compared to numerical simulations: the two are in excellent agreement.

Our analysis will parallel the theory of plasma waves, which can decay exponentially by a ''wave-particle'' resonant interaction (Landau 1946; O'Neil 1965; Briggs et al. 1970; Timofeev 1992). The analogous ''wave–fluid'' resonant interaction, central to our theory of vertical alignment, has been studied previously to understand the exponential decay of two-dimensional vortex modes (Briggs et al. 1970; Pillai and Gould 1994; Corngold 1995; Spencer and Rasband 1997; Bachman 1997; Schecter et al. 2000; Balmforth et al. 2001), and to

* The National Center for Atmospheric Research is funded by the National Science Foundation.

+ Present affiliation: Hurricane Research Division, AOML/NOAA, Miami, Florida.

Corresponding author address: Dr. David A. Schecter, NCAR/ASP, P.O. Box 3000, Boulder, CO 80307.
E-mail: daspla@ucar.edu

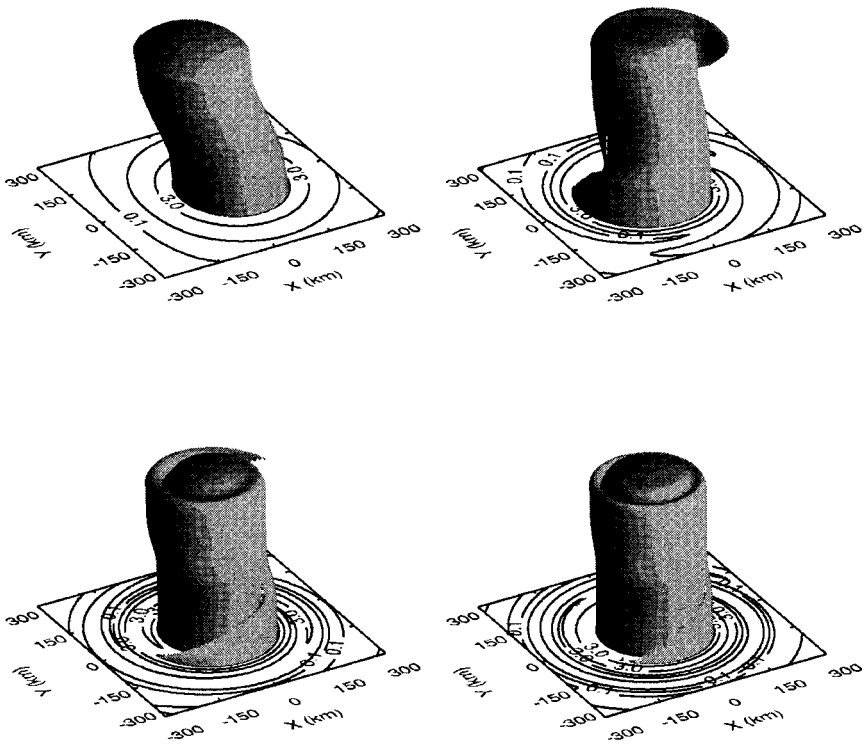

FIG. 1. Vertical alignment of a QG vortex under conservative dynamics (Reasor and Montgomery 2001, Fig. 10a). The shaded object is a PV isosurface. The bottom plane contains contours of constant PV: (top left) $t = 0$, (top right) $t = 2.7$, (bottom left) $t = 4.5$, and (bottom right) $t = 7.2$. Here, time t is measured in units of $2\pi/\Omega_o(0)$, where $\Omega_o(0)$ is the angular rotation frequency of the vortex at its center.

understand asymmetric vortex merger (Lansky et al. 1997).

In sections 5 and 6 of this article, we will examine in detail how the alignment rate of a vortex (the decay rate of a core mode) depends on the internal Rossby deformation radius l_R, defined as

$$l_R \equiv \frac{Nh}{m\pi f}. \tag{1}$$

Here, h is the height of the vortex, f is the Coriolis parameter at the latitudinal position of the vortex, N is the ambient Brunt–Väisälä frequency, and m is the number of vertical nodes in the core mode that dominates the misalignment. For a simple tilt, $m = 1$. The Brunt–Väisälä frequency measures the vertical ($\hat{z}$) stratification of the atmosphere or ocean. For atmospheres, $N^2 \equiv g\theta_o^{-1}d\theta_o/dz$, where g is gravitational acceleration and $\theta_o(z)$ is the ambient potential temperature. For oceans, $N^2 \equiv -g\rho_o^{-1}d\rho_o/dz$, where ρ_o is the ambient mass density.

The alignment rate versus l_R is not a universal curve. To illustrate this point, we will examine how the alignment rate depends on l_R for a ''Rankine-with-skirt'' vortex (section 5), and a ''Gaussian'' vortex (section 6). Rankine-with-skirt (RWS) vortices are prevalent in turbulence simulations that employ contour dynamics (Dritschel 1998). An RWS vortex can also be used to model the stratospheric polar vortex (Dritschel and Saravanan 1994). On the other hand, Gaussian vortices more closely resemble incipient tropical cyclones (for data, see Willoughby 1990). We will focus on the regime where l_R is within a factor of 10 of the radius of the vortex core. In this regime, we will show that, for the case of an RWS vortex, the alignment rate increases with increasing l_R. On the other hand, for a Gaussian vortex, the alignment rate decreases with increasing l_R.

In section 6, we will show that the core modes of a vortex disappear if l_R is reduced below a vortex-dependent threshold. Clearly, if l_R is below this threshold, the vortex can not align by the resonant damping of a mode. Rather, the vortex will align by another mechanism, such as spiral wind-up of PV (Montgomery and Kallenbach 1997; Bassom and Gilbert 1998). In this case, the misalignment generally decays nonexponentially with time.

We note that Reasor and Montgomery (2001) were the first to show that vertical alignment can occur by the decay of a core mode. This article presents a new way to understand the damping, and provides an analytical expression for the decay rate. Reasor and Montgomery (2001) analyzed the damped core mode as a packet of *freely* propagating continuum eigenmodes, with a sharply peaked frequency spectrum. From this point of view, the core mode decays by destructive in-

terference, as its constituent continuum modes disperse. Here, we view the core mode as a single wave. In this picture, the core mode decays by its *interaction* with fluid in a critical layer.

We now give an outline of the remaining text. Section 2 summarizes the quasigeostrophic fluid equations that are used to model the vortex dynamics. Section 3 reviews the properties of a Rankine vortex (uniform vortex column), which has no tendency to align (Reasor and Montgomery 2001). Section 4 explains how vortices with broader PV distributions align by the resonant damping of modes. In addition, section 4 contains a simple formula for the alignment rate. Section 5 examines the alignment of an RWS vortex. Section 6 examines the alignment of a Gaussian vortex. Section 7 recapitulates our results and discusses their relevance to the survival of incipient tropical cyclones.

2. Basic equations

a. Conservative quasigeostrophic model

The following summarizes the conservative quasigeostrophic (QG) fluid equations (e.g., Pedlosky 1987) that are used here to model the vortex dynamics. These equations are formally valid only if the Rossby number R_o is much less than unity, that is, only if the vortex rotation frequency is much less than the local Coriolis parameter f. In addition, the QG model is valid only if $h \ll L \ll r_e$, where h is the height of the vortex, L is the horizontal length scale of the vortex, and r_e is the radius of the earth. Such scale relations are satisfied by the stratospheric polar vortex, extratropical cyclones, and midlatitude oceanic eddies, but not by tropical cyclones, which have $R_o \gtrsim 1$. Quasigeostrophic theory is only a starting point for understanding tropical cyclone dynamics, as discussed in section 7.

In QG theory, there is an approximate balance between the horizontal pressure gradient and the Coriolis force. That is, the dominant component of the velocity field is given by

$$\mathbf{v}_g = \hat{z} \times \boldsymbol{\nabla}_h \psi. \tag{2}$$

Here, $\boldsymbol{\nabla}_h$ is the horizontal gradient operator, and $\psi(\mathbf{r}, t)$ is the ''geostrophic streamfunction.'' The geostrophic streamfunction is related to the pressure anomaly $p(\mathbf{r}, t)$ in the vortex, and the ambient atmospheric/oceanic density ρ_o, by the equation $\psi \equiv p/f\rho_o$.

The evolution of a QG flow is succinctly described by conservation of quasigeostrophic potential vorticity $q(\mathbf{r}, t)$ following the geostrophic flow:

$$\frac{\partial q}{\partial t} + \mathbf{v}_g \cdot \boldsymbol{\nabla}_h q = 0. \tag{3}$$

For simplicity, we assume that the mass density and the Brunt–Väisälä frequency N vary over length scales greater than the vertical extent h of the vortex. In this ''Boussinesq'' regime, the invertibility relation is given by

$$q(\mathbf{r}, t) = \nabla_h^2 \psi + \frac{f^2}{N^2} \frac{\partial^2 \psi}{\partial z^2}, \tag{4}$$

where $N \simeq$ constant.

Given suitable boundary conditions on ψ, Eqs. (2)–(4) completely describe the evolution of the horizontal flow. If the vertical velocity $v_z(\mathbf{r}, t)$ is desired, it may be obtained from the derivatives of the geostrophic streamfunction by the following:

$$\frac{\partial}{\partial t}\frac{\partial \psi}{\partial z} + \mathbf{v}_g \cdot \boldsymbol{\nabla}_h \frac{\partial \psi}{\partial z} + N^2 v_z = 0. \tag{5}$$

Equation (5) is derived from the adiabatic heat equation (Pedlosky 1987).

b. Perturbations

We now derive the conservative evolution equations for small-amplitude perturbations on a QG vortex. To begin with, we introduce a cylindrical coordinate system (r, φ, z). The PV distribution q_o and the streamfunction ψ_o of the unperturbed vortex are assumed to be independent of the vertical coordinate z and the polar angle φ.

The total PV, and the total streamfunction of the vortex can be written as follows:

$$\begin{aligned} q(r, \varphi, z, t) &= q_o(r) + \Delta q(r, \varphi, z, t), \\ \psi(r, \varphi, z, t) &= \psi_o(r) + \Delta\psi(r, \varphi, z, t), \end{aligned} \tag{6}$$

where Δq and $\Delta\psi$ are perturbations, perhaps associated with a tilt. For analysis, each perturbation field is decomposed into an azimuthally symmetric part (S), and an asymmetric part (A); that is,

$$\begin{aligned} \Delta q(r, \varphi, z, t) &= \delta q^{(S)}(r, z, t) + \delta q^{(A)}(r, \varphi, z, t), \\ \Delta\psi(r, \varphi, z, t) &= \delta\psi^{(S)}(r, z, t) + \delta\psi^{(A)}(r, \varphi, z, t). \end{aligned} \tag{7}$$

By definition, $\delta q^{(S)} \equiv (2\pi)^{-1} \int_o^{2\pi} d\varphi \Delta q$, and $\delta\psi^{(S)} \equiv (2\pi)^{-1} \int_o^{2\pi} d\varphi \Delta\psi$. The asymmetric perturbation fields satisfy $\int_o^{2\pi} d\varphi\ \delta q^{(A)} = \int_o^{2\pi} d\varphi\ \delta\psi^{(A)} = 0$.

Next, $\delta q^{(A)}$ and $\delta\psi^{(A)}$ are expanded into Fourier series in φ and z. Motivated by tropical cyclone observations (Hawkins and Rubsam 1968) and numerical simulations (Rotunno and Emanuel 1987), we will assume that the potential temperature is constant along the top and bottom surfaces of the vortex. This implies that $\partial_z \Delta\psi$ vanishes at $z = 0$ and at $z = h$. We can then write

$$\begin{aligned} &\delta q^{(A)}(r, \varphi, z, t) \\ &\quad = \sum_{m=0,n=1}^{\infty} \delta q^{(m,n)}(r, t) e^{in\varphi} \cos(m\pi z/h) + \text{c.c.}, \\ &\delta\psi^{(A)}(r, \varphi, z, t) \\ &\quad = \sum_{m=0,n=1}^{\infty} \delta\psi^{(m,n)}(r, t) e^{in\varphi} \cos(m\pi z/h) + \text{c.c.}, \end{aligned} \tag{8}$$

where ''c.c.'' denotes the complex conjugate. Both series in Eq. (8) exclude terms with $n = 0$, because such terms constitute the azimuthally symmetric parts of the perturbation fields. The cosine vertical eigenfunctions in Eq. (8) are special to the Boussinesq approximation. In the non-Boussinesq regime, similar, but less familiar, eigenfunctions replace the cosines.

Consider now the evolution of the *asymmetric* perturbation fields. If we neglect terms in Eq. (3) that are of second order in the perturbation amplitude, we obtain the following linear equation for each Fourier component of $\delta q^{(A)}$:

$$\frac{\partial}{\partial t}\delta q^{(m,n)} + in\Omega_o \delta q^{(m,n)} - \frac{in}{r} q_o' \delta\psi^{(m,n)} = 0. \qquad (9)$$

Here, $\Omega_o(r) \equiv r^{-1}\psi_o'(r)$ is the angular rotation frequency of the unperturbed vortex, and the prime denotes the radial derivative. The Fourier components of the streamfunction are obtained from Eq. (4):

$$\frac{1}{r}\frac{\partial}{\partial r} r \frac{\partial}{\partial r}\delta\psi^{(m,n)} - \left(\frac{n^2}{r^2} + \frac{1}{l_R^2}\right)\delta\psi^{(m,n)} = \delta q^{(m,n)}, \qquad (10)$$

where $l_R \equiv Nh/m\pi f$ is the internal Rossby deformation radius. The boundary conditions are $\delta\psi^{(m,n)} \to 0$ as r approaches zero and infinity.

The evolution equation for the *symmetric* part of the PV perturbation can be derived by substituting Eqs. (2) and (6)–(8) into Eq. (3), and averaging over φ. The result is

$$\frac{\partial}{\partial t}\delta q^{(S)} = -\frac{2}{r}\sum_{m,m'=0,n=1}^{\infty} n \cos\left(\frac{m\pi z}{h}\right)\cos\left(\frac{m'\pi z}{h}\right)\frac{\partial}{\partial r} \times \mathrm{Im}[\delta\psi^{(m,n)}\delta q^{(m',n)*}], \qquad (11)$$

where Im denotes the imaginary part of the quantity in square brackets, and $\delta q^{(m',n)*}$ is the complex conjugate of $\delta q^{(m',n)}$. From Eq. (11), it is clear that the evolution of the symmetric part of the PV perturbation is coupled to the asymmetric part. This is why the asymmetric part of the PV perturbation (e.g., a tilt) can decay in the absence of viscosity while, for example, total bulk kinetic energy is conserved: the energy lost by the asymmetric perturbation is absorbed by the symmetric perturbation.

3. Perpetual tilt of a compact vortex

Before discussing how a vortex vertically aligns, we review a counterexample. The simplest vortex that does not align is a Rankine vortex. The equilibrium PV distribution of a Rankine vortex is given by

$$q_o(r) = \begin{cases} Q_o & r \le r_v \\ 0 & r > r_v, \end{cases} \qquad (12)$$

where Q_o is a positive constant. For $r < r_v$ the angular rotation frequency of a Rankine vortex has the constant value $\Omega_o(r) = Q_o/2$. For $r > r_v$, the angular rotation frequency decays monotonically with r. Specifically,

$$\Omega_o(r) = \frac{Q_o}{2}\left(\frac{r_v}{r}\right)^2, \qquad r > r_v. \qquad (13)$$

A Rankine vortex supports a discrete linear eigenmode of oscillation for each asymmetric component of the PV perturbation. As shown by Reasor and Montgomery (2001), these discrete eigenmodes have the form[1]

$$\delta q^{(m,n)}(r, t) = \frac{A}{2} Q_o r_v \delta(r - r_v) e^{-i\omega t}$$

$$\delta\psi^{(m,n)}(r, t) = \frac{A}{2} Q_o r_v^2 G_{mn}(r, r_v) e^{-i\omega t}, \qquad (14)$$

where A is a dimensionless complex amplitude, ω is the eigenfrequency, and $\delta(r - r_v)$ is the Dirac delta function centered at r_v. The Green function is given by

$$G_{mn}(r, r') = -I_n(r_</l_R)K_n(r_>/l_R), \qquad (15)$$

where I_n and K_n are modified Bessel functions of the n^{th} order, and $r_>$ ($r_<$) is the larger (smaller) of r and r'. G_{mn} depends implicitly on m through l_R [Eq. (1)].

Upon substituting Eqs. (14) into Eqs. (9) and (10), one can check that the eigenfrequencies of the discrete modes of a Rankine vortex are real and given by

$$\omega = nQ_o\left[\frac{1}{2} + G_{mn}(r_v, r_v)\right]. \qquad (16)$$

The critical radius r_* of a mode is defined by the following resonance condition:

$$\Omega_o(r_*) \equiv \omega/n. \qquad (17)$$

That is, r_* is where the unperturbed fluid rotation frequency equals the angular phase velocity of the mode. Using Eqs. (13) and (16), we obtain

$$r_* = r_v[1 + 2G_{mn}(r_v, r_v)]^{-1/2} \qquad (18)$$

for the critical radius of a discrete mode of a Rankine vortex.

The modes of Eqs. (14)–(18) are examples of discrete ''vortex Rossby modes.'' Like planetary Rossby waves, they are supported by a PV gradient, q_o'. Because q_o' is negative, they are also retrograde; that is, the phase velocity ω/n of a mode is less than the angular fluid velocity Ω_o at the radius where that mode is peaked (r_v for a Rankine vortex).

In linear theory, a generic deformation of a Rankine vortex evolves as a superpositon of its discrete modes. Vertical alignment requires the decay of discrete modes

[1] The undamped discrete modes derived in QG theory for a vertically stratified Rankine vortex are similar to the discrete modes of a uniform density Rankine vortex, discussed by Kelvin (1880) and Lamb (1945).

with $n = 1$. Since the discrete modes of a Rankine vortex are undamped, a Rankine vortex will not align.

In fact, many other vortices stay misaligned because they too possess undamped discrete modes. To begin with, all vortices have undamped $n = 1$ ''pseudomodes'' in the limit of infinite l_R.[2] A pseudomode is a discrete mode with $\omega = 0$ and radial PV eigenfunction $\xi(r) \propto q_o'(r)$. The excitation of a pseudomode can be viewed as a change in the equilibrium state of the vortex; for example, a change from an upright to a tilted equilibrium.

Even if l_R is finite, there is an infinite set of ''compact'' vortices that support undamped discrete modes, with $\omega \neq 0$. By compact we mean simply that q_o is zero beyond some core radius r_v, as is the case for the Rankine vortex. Because compact vortices can support undamped discrete modes, they need not align.

Undamped discrete modes and pseudomodes share a common trait: $q_o' = 0$ at the critical radius r_*. One can easily check that $r_* > r_v$, and therefore that $q_o'(r_*) = 0$ for the discrete modes of a Rankine vortex. For a pseudomode, r_* is at infinity, where the PV and its derivatives are zero. Section 4 will explain why zero PV gradient at r_* neutralizes the decay of a discrete mode.

4. Alignment by the resonant damping of a mode

The following contains a new theory of vertical alignment. Section 4a establishes a framework for analysis, by dividing the vortex into an inner core and an outer skirt. A misalignment (e.g., a tilt) is viewed as the excitation of a discrete core mode. In general, this mode is resonant with the fluid rotation frequency at a critical radius r_* in the outer skirt. Section 4b invokes conservation of canonical angular momentum [Eq. (21)] to explain why this resonance damps the mode with time (and causes the vortex to align), provided that $q_o'(r_*) < 0$. In section 4.c, an analytical expression for the decay rate is derived. In section 4d, we show how conservation of ''wave activity'' can also explain the decay of a core mode. Readers familiar with wave activity may prefer to read section 4d before reading section 4b.

a. Vortex core and its modes

Figure 2 illustrates how a typical vortex divides into a compact core of radius r_v and an outer skirt. The unperturbed PV distribution can be written

$$q_o(r) = q_{o,c}(r) + q_{o,s}(r), \tag{19}$$

where the subscripts ''c'' and ''s'' denote core and skirt, respectively. We will only consider cases in which $q_{o,c}$ decreases monotonically with radius. The PV perturbation can also be written as a sum of core and skirt contributions: $\Delta q(r, \varphi, z, t) = \Delta q_c(r, \varphi, z, t) + \Delta q_s(r, \varphi, z, t)$. By definition, $q_{o,c} = \Delta q_c = 0$ for $r \gtrsim r_v$, and $q_{o,s} = \Delta q_s = 0$ for $r \lesssim r_v$. Note that the value of the core radius r_v is somewhat arbitrary. Precise definitions are given in sections 5 and 6 for two different vortices. For now, let it suffice to say that the bulk of the PV is contained within the core, that is, within a cylinder of radius r_v.

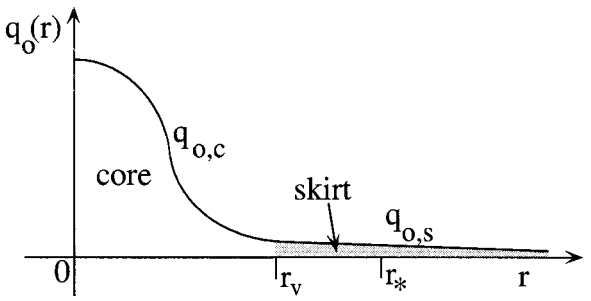

FIG. 2. A typical vortex consists of a core of radius r_v and a skirt (shaded). The core, containing the bulk of the PV, can support discrete vortex Rossby modes. The critical radius r_* of each mode is presumed to be in the skirt.

We assume that the vortex core supports discrete vortex Rossby modes of the form

$$\Delta q_c = \frac{a(t)}{2}\xi(r)e^{i(n\varphi-\omega t)}\cos\left(\frac{m\pi z}{h}\right) + \text{c.c.}, \tag{20a}$$

where ω is real. The streamfunction produced by such a mode is given by

$$\Delta\psi = \frac{a(t)}{2}\Psi(r)e^{i(n\varphi-\omega t)}\cos\left(\frac{m\pi z}{h}\right) + \text{c.c.} \tag{20b}$$

The radial eigenfunctions $\Psi(r)$ and $\xi(r)$ are related to each other by Eq. (10), with $\delta\psi^{(m,n)} \to \Psi$ and $\delta q^{(m,n)} \to \xi$. By analogy to a Rankine vortex (section 3), we may assume that the core modes are retrograde. Provided that $\Omega_o' < 0$ for all $r > 0$, this implies that the critical radius r_* [Eq. (17)] of each mode is in the skirt ($r_* > r_v$).

Unlike the discrete modes of a Rankine vortex, the core modes considered here can decay by their interactions with the skirt. Furthermore, in general, the core modes are not exact solutions to the linear eigenmode equation. For this reason, they are sometimes referred to as ''quasi modes'' (Reasor and Montgomery 2001, and references therein). As we will see, the amplitude $|a|$ of a quasi mode exhibits an early stage of exponential decay. However, in contrast to the behavior of a pure eigenmode, the amplitude of a quasi mode decays nonexponentially at late times.

[2] If l_R is infinite, there is no vertical motion, and the horizontal flow is governed by 2D Euler dynamics. The general existence of $n = 1$ pseudomodes in 2D Euler flow is pointed out in section 3 of Michalke in Timme (1967), and in Levy (1968).

b. Resonant damping

Conservation of angular momentum is often used to gain a simple understanding of two-dimensional vortex dynamics (e.g., Lansky et al. 1997; Schecter and Dubin 1999, 2001; Schecter et al. 2000). Like the two-dimensional Euler equations, the three-dimensional QG equations [(2)–(4)] conserve the canonical angular momentum P (Sutyrin et al. 1998); that is,

$$P \equiv \int dVr^2 q(r, \varphi, z, t) = \text{constant}, \qquad (21)$$

where $dV \equiv rdrd\varphi dz$, and the integral is over the entire fluid. The canonical angular momentum consists of contributions from the core and skirt of the vortex:

$$P = \int dVr^2 q_c(r, \varphi, z, t) + \int dVr^2 q_s(r, \varphi, z, t)$$
$$\equiv P_c + P_s, \qquad (22)$$

where $q_c \equiv q_{o,c} + \Delta q_c$, and $q_s \equiv q_{o,s} + \Delta q_s$. By conservation of total P, any gain of P_s is compensated by a loss of P_c. This has a simple geometrical interpretation: any increase in the (PV weighted) mean square radius of the skirt requires a decrease in the mean square radius of the core.

Suppose that at $t = 0$ a single core mode is excited. The wavenumbers of this mode are arbitrary, but for illustrative purposes we consider the specific case in which $(m, n) = (1, 1)$. This initial condition is depicted in Fig. 3a and is similar to the initial condition in Fig. 1. It is created by horizontally displacing the PV distribution at all vertical levels, such that the displacement amplitude varies with z like $\cos(\pi z/h)$. Provided that $q'_{o,c} < 0$ for all $r > 0$, this initial perturbation increases the PV-weighted mean square radius of the vortex core; that is, the perturbation increases P_c.

Figure 3a also illustrates our expectation that the mode is damped with time, due to its interaction with the skirt. We now explain why the alignment in Fig. 3a follows from conservation of total P [Eq. (22)].

To begin with, consider the flow perturbation, in the skirt, that is created by the mode. Figure 3b is a sketch of the horizontal flow in the skirt, at an arbitrary vertical level. This flow is shown in a reference frame that corotates with the mode, so that the streamlines form a ''cat's-eye'' about the critical radius r_* [Eq. (17)].

By inspection of the streamlines, one can imagine that the PV is effectively redistributed about r_*. As illustrated in Fig. 3(c), this redistribution tends to create a radial plateau about r_* in the PV distribution, averaged over φ. If $q'_{o,s}(r_*) < 0$, the formation of a plateau increases the mean square radius of the skirt and thereby increases P_s. By conservation of total P [Eq. (22)], the mean square radius of the vortex core (i.e., P_c) must decrease. This is accomplished by the decay of the core mode, that is, the decay of the tilt, as illustrated in Fig. 3a.

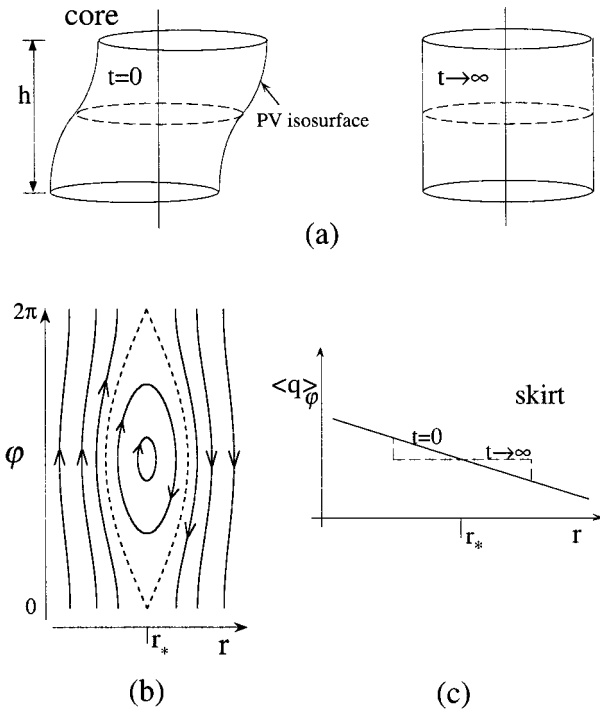

FIG. 3. (a) The (1,1) core mode is excited at $t = 0$. (b) This mode creates a cat's-eye in the streamlines in the vicinity of r_*. (c) The redistribution of PV about r_* tends to generate a plateau in $\langle q \rangle_\varphi$—the azimuthally averaged PV. This plateau increases the (PV weighted) mean square radius of the skirt. To conserve the mean square radius of the entire vortex, that is, to conserve total P, the core mode decays (a).

Note that if $q'_{o,s}(r_*) = 0$, then the redistribution of resonant PV elements (PV elements near r_*) produces no change in P_s. Consequently, there is no change in P_c, and the core mode does not decay. This is why compact vortices, which have no skirts, generally do not align. Furthermore, if $q'_{o,s}(r_*) > 0$, then the redistribution of resonant PV elements decreases P_s. In this case, the core mode grows with time; that is, the wave–fluid resonant interaction causes an instability.

In section 4c, we will show that the amplitude $|a(t)|$ of a core mode [Eqs. (20)] decays or grows exponentially with time, due to the resonance at r_*. Specifically, we will show that there is an early period during which $|a| \propto e^{\gamma t}$, where

$$\gamma = \frac{\pi n}{\langle \xi, \xi \rangle} \frac{q'_{o,s} \Psi \Psi^*}{|\Omega'_o|}\bigg|_{r_*}, \qquad (23)$$

and $\langle \xi, \xi \rangle$ is the angular pseudomomentum (total wave activity) of the core mode, defined by

$$\langle \xi, \xi \rangle \equiv -\int_0^{r_v} dr \frac{r^2}{q'_{o,c}} \xi^* \xi. \qquad (24)$$

If the vortex has a purely monotonic core, then $q'_{o,c} < 0$ and $\langle \xi, \xi \rangle$ is positive. So, in accordance with our discussion of conservation of P, γ has the same sign as $q'_{o,s}(r_*)$.

We have explained the decay of a core mode as the ''equal and opposite'' reaction to the formation of a PV plateau about a critical radius (Fig. 3c). This plateau is a nonlinear (second order) perturbation; however, the early stage of its formation, which coincides with the early exponential decay of the mode, is described by linear theory [Eqs. (9)–(10)]. This result is well known from previous studies of the resonant damping of modes in fluids and plasmas (O'Neil 1965; Briggs et al. 1970; Pillai and Gould 1994; Bachman 1997; Schecter et al. 2000; Balmforth et al. 2001).

The time at which linear theory can be expected to fail is the orbital period of a typical PV element that is trapped on a closed streamline in Fig. 3b (O'Neil 1965; Briggs et al. 1970). This orbital period is of order $2\pi/\omega_b$, where

$$\omega_b^2 = \frac{n^2}{r_*}|2\delta\psi^{(m,n)}(r_*)\Omega_o'(r_*)|. \tag{25}$$

Here, $|\delta\psi^{(m,n)}(r_*)|$ is the initial amplitude of the streamfunction perturbation, evaluated at the critical radius r_*. We expect that for times greater than $2\pi/\omega_b$, the amplitude of the core mode will ''bounce'' (begin to increase) and then equilibrate at some finite value. Experiments have demonstrated such behavior during the evolution of two-dimensional vortex modes (e.g., Schecter et al. 2000).[3] However, the nonlinear numerical simulations in this article (sections 5 and 6) run for times less than $2\pi/\omega_b$, and bouncing is not observed.

Of course, if the decay rate γ of the mode is much greater than ω_b, the closed streamlines in Fig. 3b will open before the PV elements complete their orbits. That is, if $\gamma/\omega_b \gg 1$, we expect that linear theory remains accurate forever, barring other nonlinear processes such as mode–mode interaction.

c. Weak damping

Suppose that a transient episode of external vertical shear perturbs a vortex, exciting the (m, n) discrete mode of its core. We now calculate the rate at which the core mode decays, due to a *weak* PV gradient at its critical radius r_*. We are concerned primarily with the damping of an $n = 1$ mode, since this causes vertical alignment. Nevertheless, our analysis covers all azimuthal wavenumbers. The decay of a core mode with $n \geq 2$ is associated with horizontal axisymmetrization (e.g., Schecter et al. 2000).

We obtain the decay rate of a core mode from the balance of canonical angular momentum:

$$\frac{d}{dt}P_c = -\frac{d}{dt}P_s. \tag{26}$$

The quantity $d/dt\ P_{c/s}$ is referred to as the ''torque'' on the core/skirt. The torques on the core and on the skirt are given by the following integrals:

$$\frac{d}{dt}\begin{bmatrix}P_c\\P_s\end{bmatrix} = 2\pi\int_0^h dz\int_0^\infty drr^3\frac{\partial}{\partial t}\begin{bmatrix}\delta q_c^{(S)}\\\delta q_s^{(S)}\end{bmatrix}, \tag{27}$$

where $\delta q_{c/s}^{(S)}(r, z, t)$ is the azimuthally symmetric part of the PV distribution in the core/skirt.

From Eq. (11), the time derivatives of the symmetric PV components are given approximately by

$$\frac{\partial}{\partial t}\begin{bmatrix}\delta q_c^{(S)}\\\delta q_s^{(S)}\end{bmatrix} = -\frac{2n\cos^2(m\pi z/h)}{r}\frac{\partial}{\partial r}\mathrm{Im}\begin{bmatrix}\delta\psi^{(m,n)}\delta q_c^{(m,n)*}\\\delta\psi^{(m,n)}\delta q_s^{(m,n)*}\end{bmatrix}. \tag{28}$$

Upon comparison to Eq. (11), it is clear that the right-hand side of Eq. (28) neglects asymmetries with wavenumbers (m', n') different from the wavenumbers (m, n) of the core mode. Such neglect is valid to second order in the initial perturbation amplitude. To the same order of accuracy, it is valid to use the *linear* solutions for $\delta\psi^{(m,n)}$ and $\delta q_{c/s}^{(m,n)}$ in Eq. (28).

By assumption, the PV perturbation in the vortex core $(r \lesssim r_v)$ consists entirely of a core mode [Eq. (20a)]; that is,

$$\delta q_c^{(m,n)} = \frac{a(t)}{2}e^{-i\omega t}\xi(r). \tag{29}$$

Substituting Eq. (29) into the linearized PV equation [Eq. (9)] yields

$$\delta\psi^{(m,n)} = \frac{r}{2n}\frac{\xi}{q_{o,c}'}(n\Omega_o - \omega)ae^{-i\omega t} - i\frac{r}{2n}\frac{\xi}{q_{o,c}'}\frac{da}{dt}e^{-i\omega t} \tag{30}$$

in the vortex core. Using Eqs. (29) and (30) to evaluate the time derivative of $\delta q_c^{(S)}$ [Eq. (28)], we obtain

$$\frac{\partial}{\partial t}\delta q_c^{(S)} = \frac{\cos^2(m\pi z/h)}{4r}\frac{d}{dr}\left(r\frac{\xi\xi^*}{q_{o,c}'}\right)\frac{d}{dt}|a|^2. \tag{31}$$

Using Eq. (31) to evaluate the torque [Eq. (27)] on the vortex core gives

$$\frac{d}{dt}P_c = \frac{\pi h}{2}\langle\xi, \xi\rangle\frac{d}{dt}|a|^2, \tag{32}$$

where $\langle\xi, \xi\rangle$ was previously defined by Eq. (24).

We now evaluate the torque on the skirt $(r \gtrsim r_v)$. From the linearized PV equation [Eq. (9)], we have

$$\frac{\partial}{\partial t}\delta q_s^{(m,n)} + in\Omega_o\delta q_s^{(m,n)} - in\frac{q_{o,s}'}{r}\delta\psi^{(m,n)} = 0. \tag{33}$$

We assume that the streamfunction perturbation in the skirt is dominated by the streamfunction of the core mode; that is, we let

[3] Balmforth et al. (2001) address the bouncing and equilibration of two-dimensional vortex modes in greater detail. They also demonstrate that such effects are not observed if the initial mode amplitude is below a critical value.

$$\delta\psi^{(m,n)} = \frac{a(t)}{2} e^{-i\omega t}\Psi(r) \tag{34}$$

in Eq. (33). Equation (34) makes sense only if $q'_{o,s}$ is sufficiently small. Otherwise, the redistribution of PV in the skirt with time can profoundly alter the value of $\delta\psi^{(m,n)}$ in the skirt. Substituting Eq. (34) into Eq. (33) and integrating, we obtain

$$\delta q_s^{(m,n)} = in\frac{q'_{o,s}\Psi}{2r} e^{-in\Omega_o t}\int_0^t dt' a(t') e^{i(n\Omega_o-\omega)t'}. \tag{35}$$

For simplicity, we have assumed that the PV perturbation in the skirt is initially zero. Using Eqs. (34) and (35) to evaluate the time derivative of $\delta q_s^{(S)}$ [Eq. (28)] yields

$$\frac{\partial}{\partial t}\delta q_s^{(S)} = \frac{n^2}{2r}\cos^2\left(\frac{m\pi z}{h}\right)\frac{\partial}{\partial r} \times \mathrm{Im}\left[i\frac{q'_{o,s}\Psi\Psi^*}{r}\int_0^t dt' a(t) a^*(t') e^{i(n\Omega_o-\omega)(t-t')}\right]. \tag{36}$$

Equation (36) implies that the torque [Eq. (27)] on the skirt is given by

$$\frac{d}{dt}P_s = -\pi n^2 h\,\mathrm{Im}\left[i\int_0^\infty dr q'_{o,s}\Psi\Psi^*\int_0^t dt' a(t) a^*(t') e^{i(n\Omega_o-\omega)(t-t')}\right]. \tag{37}$$

An equation for the amplitude of the core mode is found by substituting Eqs. (32) and (37) into Eq. (26). This yields

$$\frac{d}{dt}|a|^2 = \frac{2n^2}{\langle\xi,\xi\rangle}\mathrm{Im}\left[i\int_0^\infty dr q'_{o,s}\Psi\Psi^*\int_0^t dt' a(t) a^*(t') e^{i(n\Omega_o-\omega)(t-t')}\right]. \tag{38}$$

Suppose that $t \lesssim |a(da/dt)^{-1}|$. Then $a^*(t')$ is approximately $a^*(t)$ and can be pulled out of the time integral. Furthermore, suppose that $t \gg \omega^{-1}$. Then

$$\mathrm{Re}\left[\int_0^t dt' e^{i(n\Omega_o-\omega)(t-t')}\right] = \frac{\sin[(n\Omega_o-\omega)t]}{n\Omega_o-\omega} \simeq \frac{\pi}{|n\Omega'_o(r_*)|}\delta(r-r_*), \tag{39}$$

and Eq. (38) simplifies to

$$\frac{d}{dt}|a|^2 \simeq \frac{2\pi n}{\langle\xi,\xi\rangle}\left.\frac{q'_{o,s}\Psi\Psi^*}{|\Omega'_o|}\right|_{r_*}|a|^2. \tag{40}$$

The solution to this equation is $|a| \propto e^{\gamma t}$, where γ is given by Eq. (23). For a discussion of this result, we refer the reader back to section 4b. Note that Eq. (40) can hold over times much longer than $|\gamma|^{-1}$, even though our simplified derivation employed the condition that $t \lesssim |\gamma|^{-1}$. This fact is later illustrated in Figs. 6 and 8.

d. Wave activity

Sections 4b and 4c explained the damping of a core mode (i.e., vertical alignment) using conservation of canonical angular momentum P. Alternatively, one can

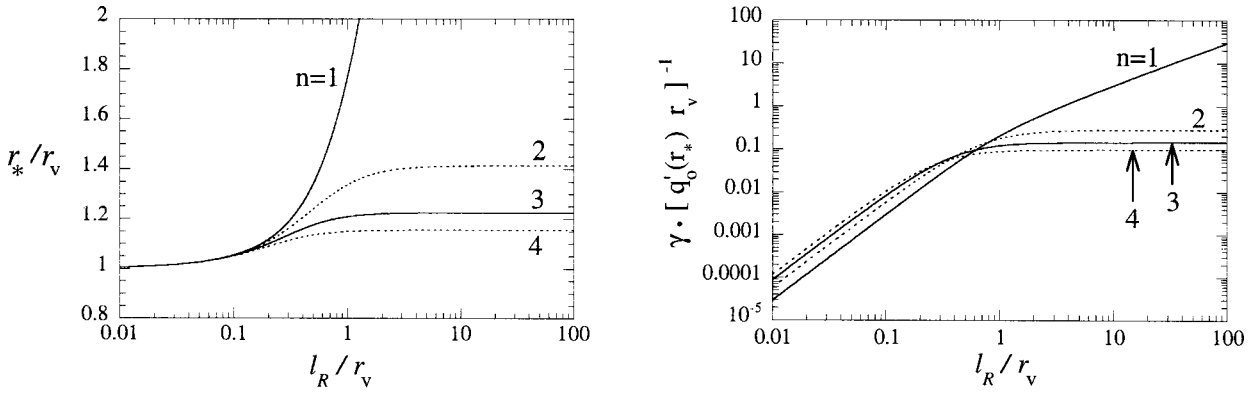

FIG. 4. Damped core modes of an RWS vortex: (a) the critical radius r_* as a function of the internal Rossby deformation radius l_R; (b) the exponential decay rate γ as a function of l_R.

explain the damping of a core mode using conservation of wave activity (e.g., Held 1985).

The linear QG model of the vortex dynamics conserves the total wave activity,

$$\mathcal{A} \equiv \int dV \frac{r}{2q_o'}(\Delta q)^2. \tag{41}$$

Here Δq is the PV perturbation, $q_o'(r)$ is the radial derivative of the unperturbed PV distribution, and the integral is over the entire fluid. For our purpose, it is convenient to express conservation of total wave activity as a balance between the rates of change of wave activity in the core and in the skirt:

$$\frac{d}{dt}\int dV \frac{r}{2q_{o,c}'}(\Delta q_c)^2 = -\frac{d}{dt}\int dV \frac{r}{2q_{o,s}'}(\Delta q_s)^2. \tag{42}$$

A discrete mode in the vortex core corresponds to a perturbation Δq_c. In time, the core mode creates a PV perturbation Δq_s in the skirt. After a few rotation periods, Δq_s is effectively concentrated about the critical radius r_* (Fig. 3c). Suppose that $q_{o,c}'(r)$ and $q_{o,s}'(r_*)$ are both negative. Then, by conservation of total wave activity [Eq. (42)], the perturbation Δq_s created at r_* necessitates a decrease in the magnitude of Δq_c, that is, a decay of the mode amplitude.

Conservation of wave activity, Eq. (42), can also replace conservation of canonical angular momentum, Eq. (26), as a starting point for a quantitative analysis of the decay rate γ. That is, after substituting the linear solutions for Δq_c and Δq_s into Eq. (42), one can derive Eq. (23) for γ.

5. Alignment of an RWS vortex

a. Analysis

This section examines the alignment of an RWS vortex. An ideal RWS vortex is simply a Rankine vortex [Eq. (12)] with a skirt attached to its edge. By assumption, the skirt provides a negligible contribution to the vortex circulation; that is,

$$2\pi \int_0^\infty dr r q_{o,s}(r) \ll \pi Q_o r_v^2. \tag{43}$$

An example of a smoothed RWS vortex (used for numerical simulations) is shown in section 5b, Fig. 5.

In section 3 [Eqs. (14)–(18)], we described the discrete modes of a Rankine vortex. The core modes of an ideal RWS vortex have the same eigenfunctions:

$$\xi(r) = Q_o r_v \delta(r - r_v) = -r_v q_{o,c}'$$
$$\Psi(r) = Q_o r_v^2 G_{mn}(r, r_v). \tag{44}$$

Here, $\xi(r)$ is the PV eigenfunction, $\Psi(r)$ is the streamfunction eigenfunction, and $\delta(r - r_v)$ is the Dirac delta function, which has units of one over length. The oscillation frequency ω and the critical radius r_* of each core mode are given approximately by Eqs. (16) and (18), respectively.

Due to the presence of the skirt, the core modes of an RWS vortex decay exponentially with time. The exponential decay rate γ is obtained by substituting Eq. (44) into Eq. (23). This yields

$$\gamma = n\pi Q_o \frac{q_{o,s}'(r_*) G_{mn}^2(r_*, r_v)}{|\Omega_o'(r_*)|}. \tag{45}$$

The following elaborates on how this decay rate varies with the azimuthal wavenumber n and with the internal Rossby deformation radius l_R. Although l_R does not appear explicitly in Eq. (45), it is implicit in the Green function G_{mn} and in the critical radius r_*. The *alignment rate* of the vortex is the decay rate γ of the $n = 1$ core mode that dominates the initial perturbation.

Before showing the full dependence of γ on l_R, we consider the limits where l_R approaches zero and infinity. The first step is to calculate the asymptotic forms of the critical radius. For small l_R, Eq. (18) reduces to

$$r_* \sim r_v + \frac{l_R}{2}, \qquad \frac{l_R}{r_v} \to 0. \tag{46}$$

That is, r_* approaches the radius of the uniform core as l_R approaches zero. Equation (46) indicates that r_* does not depend on the azimuthal wavenumber n, to first order in the asymptotic expansion about $l_R = 0$. On the other hand, for large l_R, Eq. (18) reduces to

$$r_* \sim \begin{cases} \sqrt{\dfrac{2l_R^2}{\ln(2l_R/r_v)}} & n = 1 \\ r_v\left[\dfrac{n}{n-1}\right]^{1/2} - \dfrac{r_v^3}{4l_R^2 n(n^2-1)}\left[\dfrac{n}{n-1}\right]^{3/2} & n \geq 2, \end{cases}$$

$$\frac{l_R}{r_v} \to \infty. \tag{47}$$

Equation (47) states that r_* diverges with l_R for all modes with $n = 1$. On the other hand, if $n \geq 2$, r_* asymptotes to a finite limit that is different for each n but generally greater than r_v. Figure 4a shows the full dependence of the critical radius r_* on l_R for $n = 1$, 2, 3, and 4.

Using Eqs. (46) and (47) for r_*, and Eq. (13) for $\Omega_o(r_*)$, we can obtain asymptotic expressions for the decay rate of each mode, for small and large l_R. For small l_R, Eq. (45) reduces to

$$\gamma \sim \frac{n\pi}{4e} r_v q_{o,s}'\left(r_v + \frac{l_R}{2}\right)\left(\frac{l_R}{r_v}\right)^2, \qquad \frac{l_R}{r_v} \to 0. \tag{48}$$

That is, for all n and bounded $q_{o,s}'(r_v + l_R/2)$, the decay rate vanishes as l_R approaches zero. This result is physically reasonable, since the skirt becomes shielded from the core mode as l_R becomes zero.

For large l_R, Eq. (45) reduces to

$$\gamma \sim \begin{cases} \dfrac{\pi}{4}\sqrt{\dfrac{2l_R^2}{\ln(2l_R/r_v)}}\,q'_{o,s}\left(\sqrt{\dfrac{2l_R^2}{\ln(2l_R/r_v)}}\right) & n = 1 \\ \dfrac{\pi}{4n} r_v \left[\dfrac{n-1}{n}\right]^{n-3/2} q'_{o,s}\left\{r_v\left[\dfrac{n}{n-1}\right]^{1/2}\right\} & n \geq 2, \end{cases}$$

$$\frac{l_R}{r_v} \to \infty. \tag{49}$$

For $n \geq 2$, we have omitted a small correction due to finite l_R, since it is unimportant. The pertinent result for $n \geq 2$ is that γ asymptotes to a finite value as l_R becomes infinite. This value of γ is equivalent to the decay rate that was derived in Briggs et al. (1970) and Schecter et al. (2000) for the core modes of an RWS vortex in strictly two-dimensional dynamics.

Figure 4b offers a more complete picture of how the decay rate γ depends on l_R, for $n = 1$, 2, 3, and 4. For this figure, γ was obtained from Eq. (45), using Eq. (18) for r_*, and Eq. (13) for $\Omega_o(r_*)$. The asymptotic behaviors discussed previously are evident. Note that the $n = 1$ curve does not imply that γ diverges with l_R. It appears this way, because the decay rates in Fig. 4b are divided by $q'_{o,s}(r_*)$. For $n = 1$, γ actually vanishes as l_R becomes infinite, that is, as $q'_{o,s}(r_*) \to q'_{o,s}(\infty) = 0$. Recall that in the limit of infinite l_R, all modes with $n = 1$ are undamped pseudomodes (Michalke and Timme 1967; Levy 1968).

b. Simulations

We now compare the analytical results of section 5a to several numerical simulations of the alignment of a smoothed RWS vortex, with varying l_R. Figure 5 shows the equilibrium PV distribution and angular rotation frequency of the smoothed RWS vortex that is used for our numerical simulations. Note that the core has approximately uniform PV, and that the skirt has relatively small PV. Although the exact functional form of the PV distribution is unimportant, it is given below for the sake of reproducibility. The PV distribution of the core is given by

$$q_{o,c}(r) = \begin{cases} \dfrac{Q_o}{2}\left[1 - a\tanh\left(\dfrac{r - r_v}{\delta r}\right)\right]\left(1 + b\dfrac{r_z - r}{r_z}\right) & r < r_z \\ 0 & r \geq r_z. \end{cases} \tag{50}$$

Here, $a = 1.01$, $b = 0.025$, $\delta r = r_v/30$, $r_z = 1.09r_v$, and Q_o is a constant with units of frequency ($Q_o \ll f$ for QG theory to apply). The parameter δr measures the width of the transition layer, centered at r_v, where the PV distribution drops rapidly to zero. The PV distribution of the skirt is given by

$$q_{o,s}(r) = \begin{cases} \dfrac{\varepsilon Q_o}{2}\left[1 - \tanh\left(\dfrac{r_v - r}{\delta r}\right)\right]\left(1 - \dfrac{3}{8}\dfrac{r}{r_v}\right) & r < \dfrac{8}{3}r_v \\ 0 & r \geq \dfrac{8}{3}r_v, \end{cases} \tag{51}$$

where $\varepsilon = 0.05$. Note that $q_{o,s}$ is negligible in the core. The total equilibrium PV of the vortex is $q_o = q_{o,c} + q_{o,s}$.

We now examine the evolution of a ''simple tilt.'' That is, at $t = 0$, we set

$$\delta q^{(1,1)}(r, t = 0) = C\frac{q_o(0)}{q'_o|_{\max}} q'_o(r), \tag{52}$$

where C is a real constant and $q'_o|_{\max}$ is the maximum equilibrium PV gradient. All other Fourier components of the perturbation are initialized to zero. Figures 1 and 3a show examples of vortices that have simple tilts. A simple tilt is dominated by the (1, 1) discrete mode of the vortex core. This follows intuitively from the fact that $\delta q^{(1,1)}(r, t = 0)$ [given by Eq. (52)] is exactly the radial eigenfunction $\xi(r)$ of the (1, 1) pseudomode, that is, the core mode in the limit of infinite l_R. The radial eigenfunction of the (1, 1) pseudomode is plotted below the equilibrium profile in Fig. 5.

Figure 6a shows the linear decay of the tilt, for cases in which $l_R = 0.5r_v$, $l_R = r_v$, $l_R = 1.5r_v$, and $l_R = 3r_v$. Here, the tilt is measured by the amplitude of the (1, 1) component of the perturbation streamfunction, evaluated at the core radius r_v. The solid curves are complete solutions of Eqs. (9) and (10), obtained from a numerical technique that is described in Schecter et al. (2000) and Sutyrin (1989). The dashed curves in Fig. 6a correspond to pure resonant damping; that is, $|\delta\psi(r_v, t)| \propto e^{\gamma t}$, where γ is given by Eq. (45). Early on, there is excellent agreement between pure resonant damping and the linear simulations; however, at late times, when $t \gg |\gamma|^{-1}$, the streamfunction tends toward power-law decay. Note that the damping rate (alignment rate) is zero for $l_R = 3r_v$. This is because the critical radius, $r_* = 3.44r_v$, is in the extreme outer region where $q_{o,s} = q'_{o,s} = 0$ [see Eq. (51)]. Therefore, there is no available mechanism for resonant damping.

Figure 6b shows that the linear results accurately de-

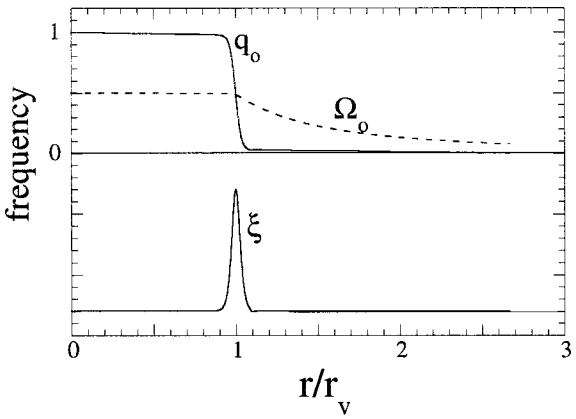

FIG. 5. The smoothed RWS vortex that is used for numerical simulations: (top) equilibrium PV profile $q_o(r)$ and angular rotation frequency $\Omega_o(r)$, normalized to $q_o(0)$; (bottom) the radial eigenfunction $\xi(r) \propto q'_o(r)$ of the $n = 1$ pseudomodes, which exist in the limit of infinite l_R. For finite l_R, the $n = 1$ core modes have approximately the same eigenfunction. The eigenfunction is zero at $r = 0$ but is offset in the figure for clarity.

scribe the vertical alignment that is observed in nonlinear simulations (diamonds). In these nonlinear simulations, the initial tilt amplitude is $C = 0.3$. The nonlinear simulations are based on a semispectral method that is described in appendix A of Reasor and Montgomery (2001). The nonlinear simulations include viscosity; however, they are terminated before viscous effects are noticeable.

We have focused on the decay of a simple tilt, in which case the vertical wavenumber m is equal to one. However, in linear theory, the decay rate depends on m only through $l_R = Nh/m\pi f$. So, the variation with l_R in Fig. 6 can also be viewed as a variation with m, keeping Nh/f fixed.

6. Alignment of a Gaussian vortex

In section 5, we examined the alignment rate of a tilted RWS vortex. We showed that a simple tilt [Eq. (52)] decays exponentially with time through the resonant damping of the (1, 1) core mode, and that the decay rate vanishes as the Rossby radius l_R approaches zero. In contrast, we now show that the alignment rate of a Gaussian vortex increases as l_R approaches zero. In addition, we show that the alignment of a Gaussian vortex occurs by the resonant damping of a core mode *only if* l_R is less than roughly one-fourth of the radius of the vortex core.

By definition, a Gaussian vortex has the following radial PV profile:

$$q_o(r) = Q_o \exp[-r^2/(2\overline{r}^2)], \tag{53}$$

where $\overline{r}$ is the PV weighted root-mean-square radius of the vortex (also the radius of maximum $|q'_o(r)|$). We define the vortex core as that part of a Gaussian vortex with $r \lesssim 3\overline{r} \equiv r_v$. In addition, we define the skirt as that part of a Gaussian vortex with $r \gtrsim r_v$. Figure 7 shows the equilibrium PV and angular rotation frequency of a Gaussian vortex. Figure 7 also shows the PV radial eigenfunction $\xi(r) \propto q'_o(r)$ of a Gaussian's $n = 1$ pseudomodes, which exist in the limit of infinite l_R. The amplitude of $\xi(r)$ is very small for $r \gtrsim r_v$; thus, we have defined the vortex core so that it contains the bulk of a pseudomode. Note that a Gaussian vortex dif-

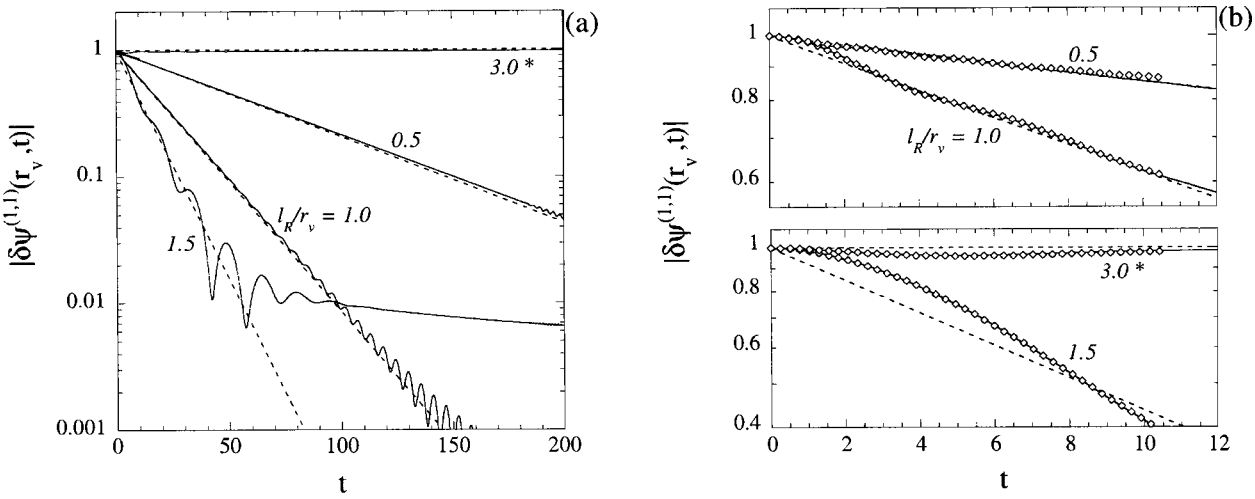

FIG. 6. (a) The exponential decay of a simple tilt on a smoothed RWS vortex (Fig. 5). The tilt of the vortex is measured by the amplitude of the (1,1) component of the streamfunction at $r = r_v$. The solid curves are complete solutions to the linear equations [Eqs. (9)–(10)]. The dashed curves correspond to the exponential decay that is predicted by the linear theory of resonant damping [Eq. (45)]. The asterisk indicates a run for which $q'_{o,s}$ is zero at the critical radius of the (1,1) core mode. (b) Comparison between linear alignment and nonlinear alignment, with initial tilt amplitude $C = 0.3$ [Eq. (52)]. The diamonds are data points from a nonlinear semispectral simulation. The linear results are the same as in (a). In both (a) and (b), time t is measured in units of $2\pi/\Omega_o(0)$, and the streamfunction amplitude is measured in units of its initial value.

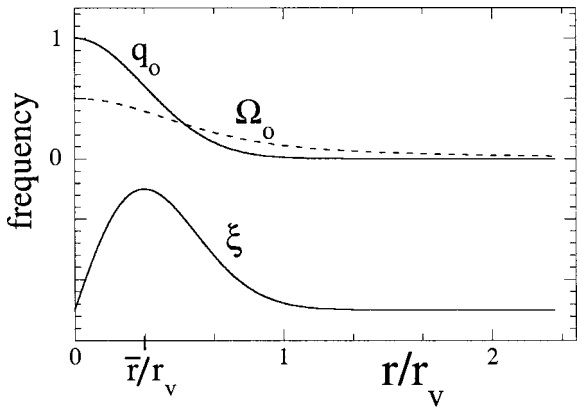

FIG. 7. A Gaussian vortex [Eq. (53)]: (top) equilibrium PV profile $q_o(r)$ and angular rotation frequency $\Omega_o(r)$, normalized to $q_o(0)$; (bottom) the radial eigenfunction $\xi(r) \propto q'_o(r)$ of the $n = 1$ pseudomodes, which exist in the limit of infinite l_R. For finite l_R, the $n = 1$ core modes have approximately the same eigenfunction. This eigenfunction is zero at $r = 0$ but is offset in the figure for clarity.

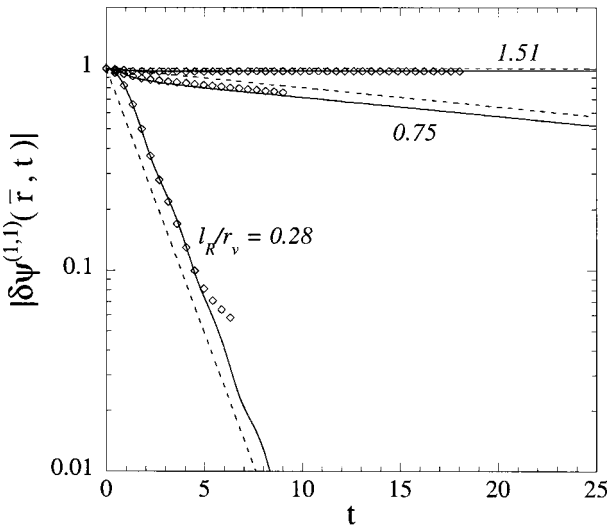

FIG. 8. The exponential decay of a simple tilt ($C = 0.3$) on a Gaussian vortex, for cases in which $l_R > r_v/4$. The tilt of the vortex is measured by the amplitude of the (1,1) component of the streamfunction at $r = \bar{r}$. The diamonds are data points from a nonlinear semispectral simulation (taken directly from Reasor and Montgomery 2001). The solid curves are complete solutions to the linear equations [Eqs. (9)–(10)]. The dashed curves correspond to the exponential decay that is predicted by the linear theory of resonant damping, that is, $|\delta\psi^{(1,1)}(\bar{r}, t)| = e^{\gamma_L t}$. Time t is measured in units of $2\pi/\Omega_o(0)$, and the streamfunction is measured in units of its initial value.

fers from an RWS vortex simply by a more gradual transition from the level of PV in the core to the level of PV in the skirt.

Suppose that at $t = 0$, a Gaussian vortex is given a simple tilt, as defined by Eq. (52). In the limit of infinite l_R, the simple tilt exclusively excites the (1, 1) pseudomode. Because this mode is undamped, the vortex remains tilted forever.

If l_R is large but finite, we expect that a simple tilt excites a (1, 1) core mode with a small frequency ω, a large critical radius $r_* > r_v$, and a spatial structure similar to that of the pseudomode (Reasor and Montgomery 2001). Because the critical radius r_* is finite, this mode can interact with the skirt effectively, that is, resonantly. Since $q'_{o,s}$ is negative, this resonant interaction should cause the mode to decay exponentially with time, as explained in section 4b.

Figure 8 shows the evolution of the perturbation streamfunction at $r = \bar{r}$ for cases in which $l_R = 0.28r_v$, $l_R = 0.75r_v$, and $l_R = 1.51r_v$. The solid curves are from numerical integrations of the linearized equations [Eqs. (9), (10)], and the diamonds are from nonlinear simulations, taken directly from Reasor and Montgomery (2001). In the nonlinear simulations, the initial tilt amplitude is $C = 0.3$.

Figure 8 clearly demonstrates that the streamfunction perturbation exhibits an early stage of exponential decay. This suggests that, even for a Gaussian vortex, the alignment process occurs through the resonant damping of a core mode. However, in contrast to the alignment rate of an RWS vortex (Fig. 5b), here the alignment rate appears to *increase* as l_R decreases toward zero.

To verify that the alignment of a tilted Gaussian vortex occurs through a wave–fluid resonant interaction, we will compare the observed decay rates in Fig. 8 to those predicted by the theory of resonant damping. The theoretical decay rates are given by Eq. (23), provided that the damping is weak, that is, $|\gamma/\omega| \ll 1$. However, to evaluate Eq. (23), we must know the eigenfunction $\xi(r)$ and the critical radius r_* of a Gaussian's core mode. We do not have an exact analytical solution to this problem. Furthermore, the damping may be strong, as for $l_R = 0.28r_v$ in Fig. 8, in which case Eq. (23) is inaccurate. So, we will use a numerical technique to find the decay rate, due to resonant damping.

A precise numerical solution is obtained by a procedure that is described in Briggs et al. (1970), Corngold (1995), Spencer and Rasband (1997), and Schecter et al. (2000). These articles discuss the resonant damping of modes on a two-dimensional vortex; however, their conclusions are readily generalized to the damping of modes on a three-dimensional vortex. In the following, we briefly describe the numerical method, without explanation. In the appendix, we explain why this method gives the decay rate of a core mode due to resonant damping.

The frequency and decay rate of a core mode are the real and imaginary parts of the complex eigenfrequency ω of the following eigenmode equation (Briggs et al. 1970; Corngold 1995; Spencer and Rasband 1997; Schecter et al. 2000):

$$\left[\frac{1}{r}\frac{\partial}{\partial r}r\frac{\partial}{\partial r} - \frac{n^2}{r^2} - \frac{1}{l_R^2} - \frac{1}{r}\frac{nq'_o}{n\Omega_o - \omega}\right]\Psi(r) = 0, \quad (54)$$

with the boundary conditions $\Psi(0) = \Psi(\infty) = 0$. An important qualification to Eq. (54) is that r is defined

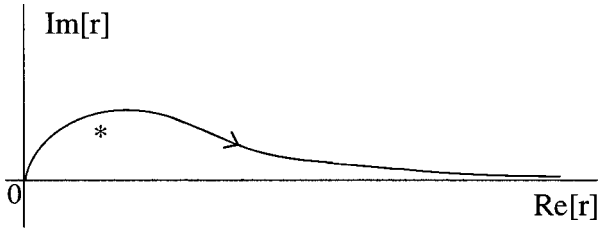

FIG. 9. Contour of radial integration that is used to uncover a Landau pole. The asterisk indicates the position where $n\Omega_o(r) = \omega_L + i\gamma_L$.

along a contour in the complex plane that arcs above the point where $n\Omega_o(r) = \omega$, as sketched in Fig. 9. If the arc is underneath this singular point, then the eigenmode problem will have no solution. The eigenfrequency is sometimes called a ''Landau pole,'' after L. Landau, who used a similar technique to calculate the damping rate of plasma waves (Landau 1946). We will denote the real and imaginary parts of the Landau pole by ω_L and γ_L, respectively.

Figure 10 illustrates the l_R dependence of the $n = 1$ Landau pole of a Gaussian vortex. This Landau pole was obtained from a numerical ''shooting'' solution to Eq. (54). Figure 10a shows that the critical radius r_*, defined by $n\Omega_o(r_*) \equiv \omega_L$, increases monotonically with l_R. This implies that the eigenfrequency ω_L decreases monotonically with l_R. On the other hand, Fig. 10b shows that the predicted decay rate γ_L is a nonmonotonic function of l_R, peaked at about $0.13r_v$.

The imaginary part (γ_L) of the Landau pole should be consistent with Eq. (23) in the regime of weak damping. To evaluate Eq. (23), we use the critical radius r_* obtained from ω_L. In addition, we use $r_v q_o'(r)$ as a good approximation for the radial eigenfunction $\xi(r)$. Finally, we use $\Psi(r_*) = \int_o^\infty drrG_{mn}(r_*, r)\xi(r)$, where G_{mn} is defined by Eq. (15). The result is shown as a dashed curve in Fig. 10b. For l_R greater than about $r_v/2$, in which case $\gamma_L/\omega_L \leq 0.1$, there is excellent agreement between γ_L and Eq. (23).

We now return to Fig. 8. The dashed curves in Fig. 8 show exponential decay, given solely by the Landau pole; that is, $|\delta\psi(\bar{r}, t)| \propto e^{\gamma_L t}$, where γ_L is obtained from Fig. 10b. There is excellent agreement between this pure resonant damping and the simulations. Of course, at later times (not shown), the amplitude exhibits power-law decay, in accord with time-asymptotic linear theory.

For all cases in Fig. 8, the critical radius is outside or at the edge of the vortex core; that is, $r_* \gtrsim r_v$. So for all cases in Fig. 8, there is a spatial separation between the core mode and the critical layer. We now consider the alignment of a Gaussian vortex, in an atmosphere or ocean with $l_R \lesssim r_v/4$. In this regime the critical radius r_* is well within the core. So the picture of a core mode interacting with a skirt breaks down and, as we will see, γ_L does not accurately give the alignment rate.

Figure 11 shows the evolution of the perturbation streamfunction at $r = \bar{r}$, for the case in which $l_R = 0.1r_v$ and $r_* = 0.24r_v$. The solid curve is from a numerical integration of the linearized equations [Eqs. (9)–(10)], and the diamonds are from a numerical integration of the nonlinear equations. The dashed curve shows the exponential decay that is given solely by the Landau pole; that is, $|\delta\psi(\bar{r}, t)| \propto e^{\gamma_L t}$, where γ_L is obtained from Fig. 10b. It is evident that the simulations do not agree with the dashed curve; that is, the alignment observed in the simulations is not explained by the resonant damping of a core mode.

Furthermore, when $l_R \lesssim r_v/4$, the PV perturbation in a Gaussian's core does not resemble a damped mode in any way. Figure 12a shows the linear evolution of the PV perturbation for the case in which $l_R = 0.1r_v$. The solid curves give the amplitude of the perturbation, whereas the dash–dot curves give the phase. Figure 12a indicates that the peak amplitude of the PV perturbation propagates radially outward, from $r = 0.33r_v$ to $r \simeq 0.4r_v$. In addition, the PV perturbation undergoes ''spiral wind-up;'' that is, it develops rapid phase oscillations in the radial direction. In Reasor and Montgomery (2001), a PV perturbation with such features is referred

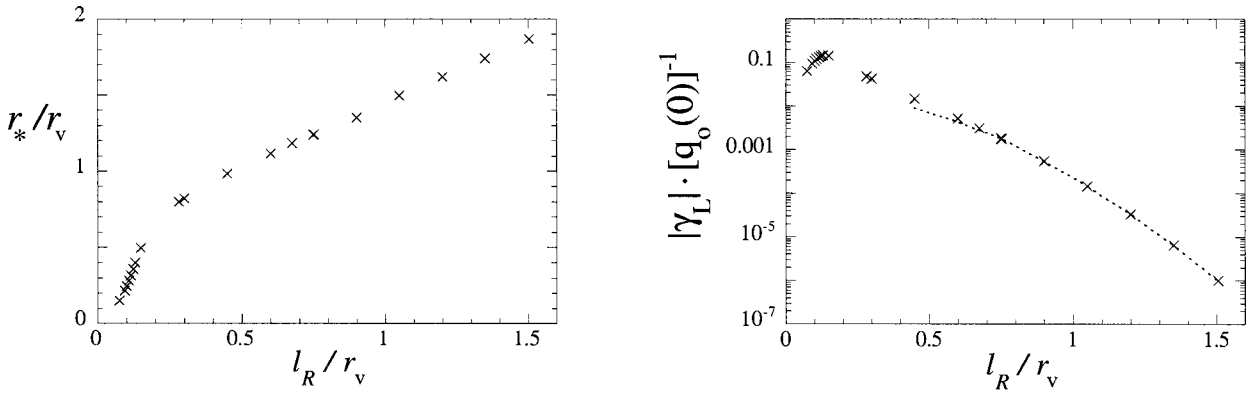

FIG. 10. Damped core modes of a Gaussian vortex: (a) the $n = 1$ critical radius r_* as a function of the internal Rossby deformation radius l_R; (b) the $n = 1$ decay rate γ_L as a function of l_R. The dashed line is Eq. (23), as explained in the text.

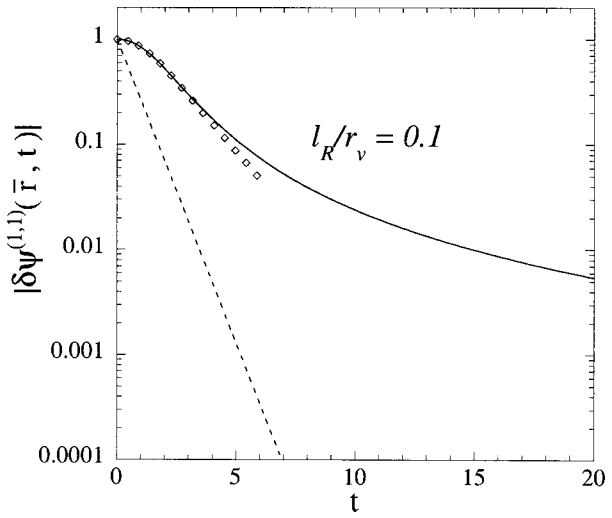

FIG. 11. The nonexponential decay of a simple tilt on a Gaussian vortex, for a case in which $l_R < r_v/4$. The tilt of the vortex is measured by the amplitude of the (1,1) component of the streamfunction at $r = \bar{r}$. The solid curve is a complete solution to the linear equations [Eqs. (9)–(10)]. The diamonds are data points from a nonlinear simulation. The dashed curve corresponds to the exponential decay that is predicted by the linear theory of resonant damping, that is, $|\delta\psi^{(1,1)}(\bar{r}, t)| = e^{\gamma_L t}$.

to as a *sheared* vortex Rossby wave. Detailed discussions of sheared vortex Rossby waves, in the analogous two-dimensional problem, can be found in Montgomery and Kallenbach (1997) and Bassom and Gilbert (1998).

In contrast, Fig. 12b shows the evolution of the PV perturbation for the case in which $l_R = 0.75r_v$, and the critical radius, $r_* = 1.24r_v$, is in the skirt. As before, the solid curves give the amplitude of the perturbation, whereas the dash–dot curves give the phase. As expected, the PV perturbation behaves like a damped mode in the vortex core. The short-dashed curves correspond to the theoretical behavior of this mode: $\delta q^{(1,1)}(r, t) \simeq a_o q_o'(r) e^{\gamma_L t - i\omega_L t}$. Here, the constant a_o is determined by a fit at $t = 4$ central rotation periods, at which point $\delta\psi^{(1,1)}(\bar{r}, t)$ (Fig. 8) begins to decay at an exponential rate. In addition, we have used $\xi(r) \simeq r_v q_o'(r)$. Figure 12b validates our assertion that a vortex aligns by the resonant damping of a core mode, provided that r_* is in the skirt.

We have demonstrated that a Gaussian vortex supports a (1, 1) discrete core mode only if $l_R \gtrsim r_v/4$, or equivalently if $1 \lesssim 4Nh/\pi f r_v$. More generally, an $n = 1$ core mode with vertical wavenumber m exists only if $m \lesssim 4Nh/\pi f r_v$. Therefore, resonant damping of a core mode can explain the alignment of a Gaussian vortex only if the dominant vertical wavenumber of the misalignment satisfies $m \lesssim 4Nh/\pi f r_v$.

Note also that for an ideal RWS vortex, where $q_{o,c}' \propto \delta(r - r_v)$, the critical radius r_* (for any n) is greater than the radius of the vortex core r_v for all values of l_R. This suggests, in contrast to the Gaussian vortex, that an ideal RWS vortex can align at an exponential rate by the resonant damping of a core mode at any level of atmospheric/oceanic stratification, and for any vertical wavenumber m that characterizes the misalignment.

7. Discussion

a. Recap

We have presented an important conservative mechanism for the vertical alignment of a QG vortex—the

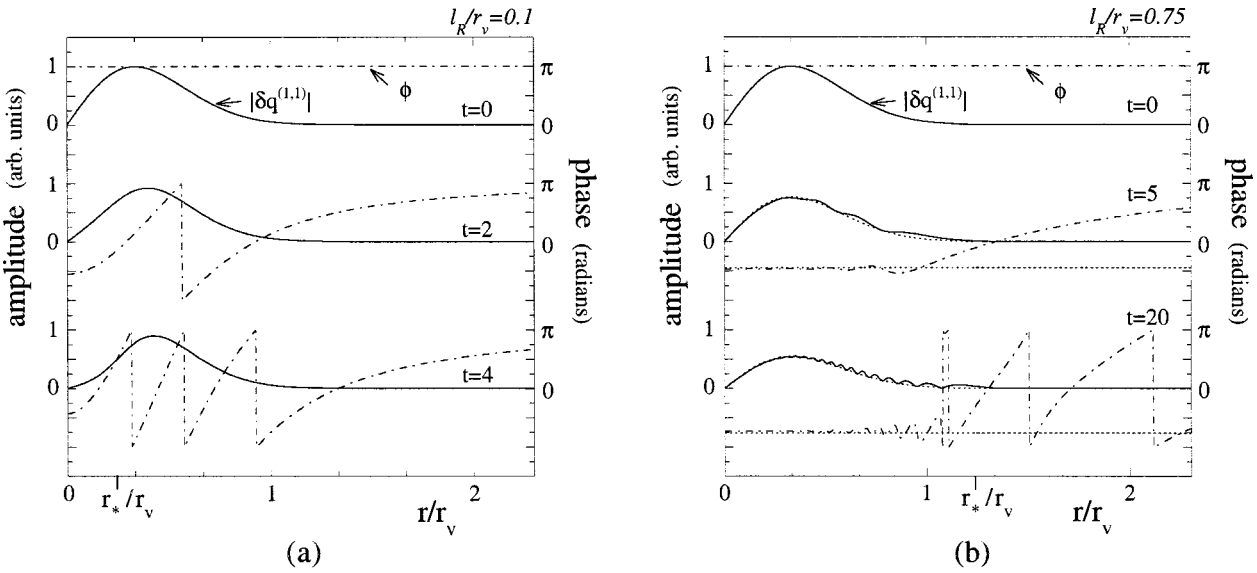

FIG. 12. Linear evolution of the PV perturbation, during the alignment of a Gaussian vortex: $\delta q^{(1,1)}(r, t) = |\delta q^{(1,1)}(r, t)| e^{i\phi(r,t)}$. (a) If r_* is far inside the vortex core, the PV perturbation does not resemble a damped mode; rather, it develops an increasing number of radial phase oscillations. (b) If r_* is in the skirt, the PV perturbation in the core behaves like an exponentially damped mode. The short-dashed curves give the behavior of the mode, as predicted by the theory of resonant damping. Time t is measured in units of $2\pi/\Omega_o(0)$.

TABLE 1. Estimated tropical cyclone parameters.

Tropical cyclone	Lat	$V(r_{mw})$ (m s^{-1})	r_{mw} (km)	$R_o(r_{mw})$	$l_R^{(QG)}/r_v$	$l_R^{(AB)}/r_v$
Danny	27°N	20	60	5	3	0.3
Arthur	16°N	10	80	3.5	4	0.5
Isabel	29°N	20	60	4.7	3	0.3
Elena 1	25°N	23	75	5	3	0.3

resonant damping of a vortex Rossby mode. In this picture, a misalignment corresponds to the weak excitation of an $n = 1$ discrete mode of the vortex core. If there is no PV gradient at the critical radius r_* [Eq. (17)], then the mode amplitude remains constant; that is, the vortex stays misaligned forever. However, even a slight negative PV gradient at the critical radius causes the mode to decay exponentially, and the vortex to align, by a wave–fluid resonant interaction (section 4).

In sections 5 and 6, we examined the alignment of an RWS vortex and a Gaussian vortex, respectively. In both cases, we showed that the theory of resonant damping accurately predicts the alignment observed in numerical simulations (Figs. 6, 8), provided that l_R is sufficiently large. At the end of section 6, we argued that, for an ideal RWS vortex, resonant damping can explain the alignment for all l_R. However, for a Gaussian vortex, we showed explicitly that the theory of resonant damping fails to explain alignment when $l_R \lesssim r_v/4$. This is because the core of a Gaussian vortex does not support an $n = 1$ discrete mode when $l_R \lesssim r_v/4$.

b. Resonant damping during tropical cyclogenesis?

To survive its early stages of development, a tropical cyclone (TC) must counter the destructive influence of external vertical shear. Moist convection likely assists in keeping TCs vertically aligned. However, they may also benefit from conservative alignment mechanisms, such as the resonant damping of a core vortex Rossby mode.

Suppose that a transient episode of external vertical shear misaligns a weak TC. Presumably, this vortex can better resist the next episode if it rapidly realigns. In QG theory, if the perturbation is dominated by a discrete vortex Rossby mode of the core, then the alignment rate (due to resonant damping) increases with the magnitude of the PV gradient at the critical radius r_* of that mode. So, with a larger (negative) PV gradient at r_*, the vortex has a better chance to survive episodes of external vertical shear and develop into a violent storm.

Of course, alignment by resonant damping can occur only if the vortex core supports a discrete $n = 1$ mode. This depends on the form of the vortex, and on the internal Rossby deformation radius l_R. Figure 13 (Willoughby 1990) shows the azimuthal velocity profiles of four weak TCs. In each case, the azimuthal velocity $V(r)$ decays more slowly than $1/r$ past the radius of maximum wind, r_{mw}. Therefore, in each case there exists a significant amount of cyclonic vorticity beyond r_{mw}. In this sense, the TCs resemble Gaussian vortices more than RWS vortices. In analogy to the QG theory of Gaussian vortices, we expect that TCs support $n = 1$ core modes if $l_R \gtrsim r_v/4$.

On the other hand, the QG equations [Eqs. (2)–(5)] are reasonable only if the Rossby number

$$R_o \equiv \frac{V(r)}{fr} \tag{55}$$

is everywhere much less than unity. To evaluate R_o, we use $f = 2\Omega_e \sin(\lambda)$, where $\Omega_e = 7.29 \times 10^{-5}$ s^{-1} is the angular rotation frequency of the earth, and λ is the latitudinal position of the vortex. Table 1 indicates that $R_o(r_{mw})$ is actually greater than unity for all of the TCs in Fig. 13. Therefore, using QG theory to understand the behavior of TCs, even weak TCs, is debatable. Nevertheless, TCs may still align in part by the resonant damping of modes.

The asymmetric balance (AB) theory of Shapiro and Montgomery (1993) includes the effects of finite R_o. The AB equations are similar to the QG equations, but the constant Rossby radius of QG theory is replaced by the following radially dependent Rossby radius:

$$l_R^{(AB)} = \frac{Nh}{m\pi\sqrt{\eta(r)\Xi(r)}} \sim \frac{Nh}{m\pi f(1 + 2R_o)}. \tag{56}$$

Here, $\eta(r)$ is the local absolute vorticity of the unperturbed vortex, and $\Xi(r)$ is the average absolute vorticity within the radius r; that is,

$$\eta(r) \equiv f + \frac{1}{r}\frac{d}{dr}rV(r), \qquad \Xi(r) \equiv f + 2\frac{V(r)}{r}. \tag{57}$$

According to Eq. (56), the Rossby radius of AB theory equals $l_R^{(QG)}$ [Eq. (1)] times f over the geometric mean of η and Ξ.

At present, we anticipate that AB dynamics has the same qualitative dependence on the average value of $l_R^{(AB)}$ that QG dynamics has on $l_R^{(QG)}$. Specifically, we expect that if $l_R^{(AB)} \gtrsim r_v/4$, the cores of the Gaussian-like TCs in Fig. 13 support $n = 1$ discrete vortex Rossby modes, which decay by resonant damping. Using $m = 1$, $h \simeq 8$ km, $N \simeq \sqrt{1.2} \times 10^{-2}$ s^{-1}, and $r_v \simeq 2r_{mw}$, we obtain values of $l_R^{(AB)}/r_v$ between 0.3 and 0.5 (see Table 1). So, the TCs in Fig. 13 are candidates to support $n = 1$ core modes, and align by resonant damping. Future work will clarify the conditions for discrete core modes to exist (if at all) for vortices with $R_o \gtrsim 1$.

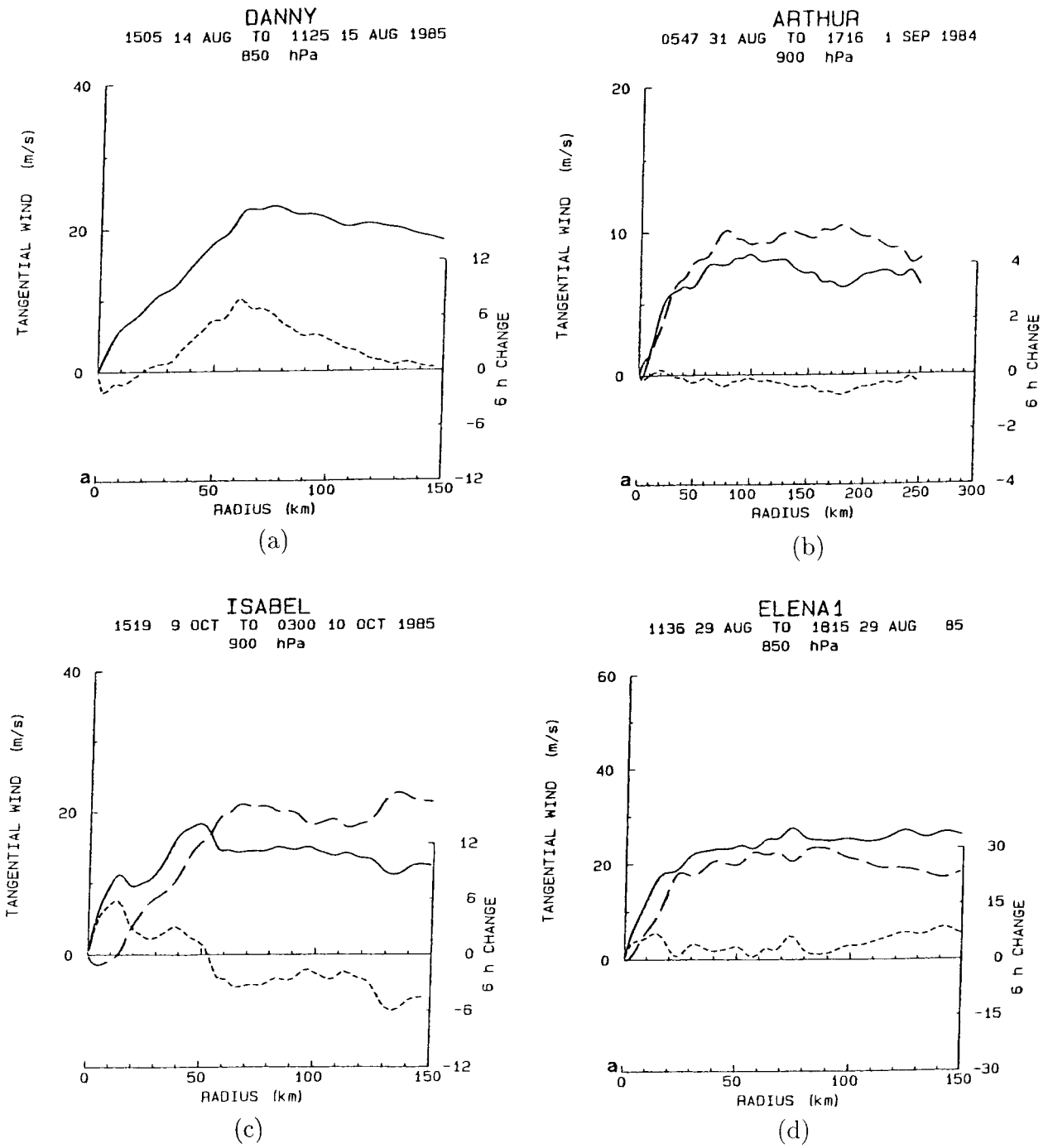

FIG. 13. Four incipient tropical cyclones (Willoughby 1990). The long-dashed and solid curves show the azimuthal (tangential) wind velocity at an early and later stage of development, respectively. The short-dashed curve represents the change in azimuthal velocity over a 6-h interval. In each case, the azimuthal wind velocity decays with radius slower than $1/r$, indicating that there exists a significant amount of cyclonic vorticity beyond the radius of maximum wind. In this sense, the tropical cyclones resemble Gaussian vortices (section 6) more than RWS vortices (section 5). (a) Danny and (d) Elena intensified into hurricanes (not shown), whereas (b) Arthur and (c) Isabel did not.

Future work will also examine how the alignment rate changes when the initial perturbation is more complicated than the simple tilt that is defined by Eq. (52). For example, convection in the core of a TC can excite single cluster PV anomalies, as described by Montgomery and Enagonio (1998), and Reasor and Montgomery (2001). These spatially concentrated PV anomalies can have a negligible overlap with discrete modes of the vortex core and behave like a superposition of sheared, radially propagating vortex Rossby waves (Montgom-

ery and Kallenbach 1997; Bassom and Gilbert 1998). Accordingly, the perturbation streamfunction would quickly exhibit power-law decay with time, in contrast to the exponential decay that is associated with resonant damping of a core mode.

Finally, we have considered an ideal scenario in which the vortex is free of environmental stress during its alignment. In reality, the vortex may experience sustained forcing (as in Jones 1995). Future work will address the effect of such forcing on the resonant damping of core modes.

Acknowledgments. D. A. Schecter thanks Dr. R. Rotunno and Dr. R. Saravanan for their helpful comments. This work was funded in part by NSF Grants ATM-9732678 and ATM-0101781.

APPENDIX

The Landau Pole

In this appendix we will describe the Laplace transform solution of the linearized perturbation equations [Eqs. (9)–(10)]. In doing so, we will explain why the Landau pole (section 6) gives the frequency and decay rate of a core mode.

Briggs et al. (1970; hereafter BDL) described the Laplace transform solution for the particular case of infinite l_R (the two-dimensional limit). We will not repeat their detailed analysis; rather, we will summarize their solution in a form that is suitable for the more general case of finite l_R. For an extended discussion, we recommend that the interested reader consult BDL and several follow-up articles (Corngold 1995; Spencer and Rasband 1997; Schecter et al. 2000). In BDL, subtleties are discussed that for the sake of brevity, we omit from our presentation.

To begin with, we introduce the temporal Laplace transform of a Fourier component of the streamfunction perturbation:

$$\delta\psi(r, t) = -\frac{1}{2\pi}\int_{+\infty+i\alpha}^{-\infty+i\alpha} d\omega\widehat{\delta\psi}(r, \omega)e^{-i\omega t}, \quad \text{(A1)}$$

$$\widehat{\delta\psi}(r, \omega) = \int_0^\infty dt\delta\psi(r, t)e^{i\omega t}. \quad \text{(A2)}$$

We have dropped the superscript (m, n) to simplify notation. In addition, α is a positive real number, so that the inverse transform is over a straight line, from right to left, in the upper-half of the complex-ω plane. Note that the inverse transform in BDL is in the lower half of the complex-ω plane: the present convention is chosen to be consistent with the articles that have followed BDL (Corngold 1995; Spencer and Rasband 1997; Schecter et al. 2000).

Upon transforming the linearized equations [Eqs. (9)–(10)], we obtain the following differential equation for $\widehat{\delta\psi}$:

$$\mathcal{L}_\omega\widehat{\delta\psi} = -i\frac{\delta q(r, t = 0)}{n\Omega_o - \omega}, \quad \text{(A3)}$$

where $\delta q(r, t = 0)$ is the initial PV perturbation, and

$$\mathcal{L}_\omega \equiv \frac{1}{r}\frac{\partial}{\partial r}r\frac{\partial}{\partial r} - \frac{n^2}{r^2} - \frac{1}{l_R^2} - \frac{1}{r}\frac{nq_o'}{n\Omega_o - \omega}. \quad \text{(A4)}$$

Equation (A3) can be solved formally with a Green function technique; that is,

$$\widehat{\delta\psi}(r, \omega) = -i\int_0^\infty dr'r'\chi(r, r')\frac{\delta q(r', t = 0)}{n\Omega_o(r') - \omega}. \quad \text{(A5)}$$

The Green function χ is given by

$$\chi(r, r') = \frac{\Psi_1(r_<)\Psi_2(r_>)}{r'W(r', \omega)}. \quad \text{(A6)}$$

Here, $r_>$ ($r_<$) is the greater (smaller) of r and r'. In addition, Ψ_1 and Ψ_2 are solutions to the homogeneous equation $\mathcal{L}_\omega\Psi_i = 0$, with the end-point conditions $\Psi_1(0) = 0$ and $\Psi_2(\infty) = 0$. The function $W(r', \omega)$ is the Wronskian determinant, defined by $W \equiv \Psi_1\Psi_2' - \Psi_1'\Psi_2$.

The Wronskian determinant is zero at values of ω for which $\Psi_1 = \Psi_2$. That is, $W = 0$ at an eigenfrequency of the following eigenmode problem:

$$\mathcal{L}_\omega\Psi(r) = 0, \qquad \Psi(0) = \Psi(\infty) = 0. \quad \text{(A7)}$$

Suppose that the vortex is purely monotonic ($q_o' < 0$ for all $r > 0$). Then the eigenmode problem [Eqs. (A7)], defined along the real-r axis, generally has no solution. On the other hand, if r defines a contour (e.g., Fig. 9) that arcs sufficiently far above the real-r axis, an eigenfrequency will emerge (Briggs et al. 1970; Corngold 1995; Spencer and Rasband 1997; Schecter et al. 2000). This eigenfrequency is a pole of $\widehat{\delta\psi}(r, \omega)$, provided that the contour of integration in (A5) is deformed appropriately into the upper half of the complex-r' plane.

As in the main text (section 6), we will denote the real and imaginary parts of this Landau pole by ω_L and γ_L, respectively. The inversion contour in Eq. (A1) can be made to wrap around the Landau pole, producing a component of $\delta\psi(r, t)$ that varies like $\Psi_L(r)e^{\gamma_L t - i\omega_L t}$. For a purely monotonic vortex, γ_L is negative, and the Landau pole contribution behaves like an exponentially damped mode. We emphasize that the location of the Landau pole is a property of the equilibrium profile, as opposed to the initial PV perturbation.

The ''eigenfunction'' $\Psi_L(r)$ generally has a discontinuity at the critical radius r_*, defined by $n\Omega_o(r_*) = \omega_L$ (Briggs et al. 1970). This discontinuity becomes negligible as γ_L approaches zero. Of course, the complete solution to $\delta\psi(r, t)$ is smooth. The smoothness is restored by an additional and essential contribution to $\delta\psi$, referred to as the ''continuum,'' or ''branch-cut'' contribution. The continuum contribution decays as a power law at late times and therefore eventually dominates the exponentially damped contribution from the Landau pole.

We now calculate the Landau pole of a vortex that consists of a core of radius r_v, and a skirt of relatively small PV [Fig. 2]. By assumption, the vortex core would support an undamped discrete mode in the absence of the skirt. This ''root mode'' satisfies the same eigenvalue problem [Eq. (A7)] that is used to calculate the Landau pole of the entire vortex, with $q_o' \to q_{o,c}'$. So, to zero order in $q_{o,s}'$, the Landau pole is the real frequency of the root mode.

If $q_{o,s}' \neq 0$, the Landau pole has an imaginary part, γ_L. To obtain an expression for γ_L, we first multiply the eigenvalue equation by $r\Psi^*(r)$ and then integrate over r:

$$\int_L dr r\Psi^* \mathcal{L}_\omega \Psi = 0. \tag{A8}$$

Here, L denotes a ''Landau contour'' that extends along the real-r axis from zero to infinity, except near r_*, where it must arc just above the point at which $n\Omega_o(r) = \omega_L + i\gamma_L$. Since $q_{o,s}'$ and γ_L are small, we may approximate Eq. (A8) with the following:

$$\int_0^\infty dr r\left[\frac{\partial\Psi^*}{\partial r}\frac{\partial\Psi}{\partial r} + \left(\frac{n^2}{r^2} + \frac{1}{l_R^2}\right)\Psi^*\Psi\right] + \left(1 + i\gamma_L\frac{d}{d\omega_L}\right)P\int_0^\infty dr\frac{nq_o'(r)\Psi^*\Psi}{n\Omega_o - \omega_L} + i\pi\frac{q_{o,s}'\Psi^*\Psi}{|\Omega_o'|}\Bigg|_{r_*} = 0. \tag{A9}$$

Here, $\Psi(r)$, ω_L, and r_* are the eigenfunction, eigenfrequency, and critical radius of the root mode, respectively. Furthermore, P denotes the principal part of the integral. In deriving Eq. (A9), we used the Plemelj formula (Muskhelishvili 1953) and the boundary conditions $\Psi(0) = \Psi(\infty) = 0$.

Equating the imaginary part of Eq. (A9) to zero, we obtain

$$\gamma_L = -\pi\frac{q_{o,s}'\Psi^*\Psi}{|\Omega_o'|}\Bigg|_{r_*}\left[\int_0^{r_v} dr\frac{nq_{o,c}'\Psi^*\Psi}{(n\Omega_o - \omega_L)^2}\right]^{-1}. \tag{A10}$$

Here, we have truncated the principal part of the integral at r_v, since the skirt contribution (multiplied by γ_L) is negligible. In section 4, we obtained an expression [Eq. (23)] for the decay rate that involved the vorticity eigenfunction $\xi(r)$ of the root mode of the vortex core. This vorticity eigenfunction is related to $\Psi(r)$ by the equation

$$\xi = \frac{nq_{o,c}'\Psi}{r(n\Omega_o - \omega_L)}, \tag{A11}$$

for r within the core. For r beyond the core, $\xi(r) = 0$. Substituting this result into Eq. (A10), we obtain

$$\gamma_L = \pi n\langle\xi, \xi\rangle^{-1}\frac{q_{o,s}'\Psi^*\Psi}{|\Omega_o'|}\Bigg|_{r_*}, \tag{A12}$$

where $\langle\xi, \xi\rangle \equiv -\int_o^{r_v} dr\, r^2\xi^*\xi/q_{o,c}'$. Equation (A12) is the same as Eq. (23).

REFERENCES

Bachman, D. A., 1997: Nonlinear phenomena in a pure electron plasma studied with a 2D fluid code. Ph.D. dissertation, California Institute of Technology, 143 pp.

Balmforth, N. J., S. G. Llewellyn Smith, and W. R. Young, 2001: Disturbing vortices. *J. Fluid Mech.,* **426,** 95–133.

Bassom, A. P., and A. D. Gilbert, 1998: The spiral wind-up of vorticity in an inviscid planar vortex. *J. Fluid Mech.,* **371,** 109–140.

Briggs, R. J., J. D. Daugherty, and R. H. Levy, 1970: Role of Landau damping in crossed-field electron beams and inviscid shear flow. *Phys. Fluids,* **13,** 421–432.

Corngold, N. R., 1995: Linear response of the two-dimensional pure electron plasma: Quasi-modes for some model profiles. *Phys. Plasmas,* **2,** 620–628.

Dritschel, D. G., 1998: On the persistence of non-axisymmetric vortices in inviscid two-dimensional flows. *J. Fluid Mech.,* **371,** 141–155.

——, and R. Saravanan, 1994: Three-dimensional quasi-geostrophic contour dynamics, with an application to stratospheric vortex dynamics. *Quart. J. Roy. Meteor. Soc.,* **120,** 1267–1297.

Hawkins, H. F., and D. T. Rubsam, 1968: Hurricane Hilda, 1964: II. The structure and budgets of the hurricane on October 1, 1964. *Mon. Wea. Rev.,* **96,** 617–636.

Held, I. M., 1985: Pseudomomentum and the orthogonality of modes in shear flows. *J. Atmos. Sci.,* **42,** 2280–2288.

Jones, S. C., 1995: The evolution of vortices in vertical shear. I: Initially barotropic vortices. *Quart. J. Roy. Meteor. Soc.,* **121,** 821–851.

Kelvin, Lord, 1880: On the vibrations of a columnar vortex. *Phil. Mag.,* **10,** 155.

Lamb, Sir H., 1945: *Hydrodynamics.* 6th ed. Dover, 231 pp.

Landau, L., 1946: On the vibration of the electronic plasma. *J. Phys. U.S.S.R.,* **10,** 25.

Lansky, I. M., T. M. O'Neil, and D. A. Schecter, 1997: A theory of vortex merger. *Phys. Rev. Lett.,* **79,** 1479–1482.

Levy, R. H., 1968: Two new results in cylindrical diocotron theory. *Phys. Fluids,* **11,** 920–921.

Michalke, A., and A. Timme, 1967: On the inviscid instability of certain two-dimensional vortex-type flows. *J. Fluid Mech.,* **29,** 647–666.

Montgomery, M. T., and R. J. Kallenbach, 1997: A theory of vortex Rossby-waves and its application to spiral bands and intensity changes in hurricanes. *Quart. J. Roy. Meteor. Soc.,* **123,** 435–465.

——, and J. Enagonio, 1998: Tropical cyclogenesis via convectively forced vortex rossby waves in a three-dimensional quasigeostrophic model. *J. Atmos. Sci.,* **55,** 3176–3207.

Muskhelishvili, N. I., 1953: *Singular Integral Equations.* 2d ed. Dover, 447 pp.

O'Neil, T. M., 1965: Collisionless damping of nonlinear plasma oscillations. *Phys. Fluids,* **8,** 2255–2262.

Pedlosky, J., 1987: *Geophysical Fluid Dynamics.* Springer-Verlag, 710 pp.

Pillai, S., and R. W. Gould, 1994: Damping and trapping in 2D inviscid fluids. *Phys. Rev. Lett.,* **73,** 2849–2852.

Polvani, L. M., 1991: Two-layer geostrophic vortex dynamics. Part 2: Alignment and two-layer V-states. *J. Fluid Mech.,* **225,** 241–270.

Reasor, P. D., and M. T. Montgomery, 2001: Three dimensional alignment and corotation of weak, TC-like vortices via linear vortex Rossby waves. *J. Atmos. Sci.,* **58,** 2306–2330.

Rotunno, R., and K. A. Emanuel, 1987: An air–sea interaction theory for tropical cyclones. Part II: Evolutionary study using a nonhydrostatic axisymmetric numerical model. *J. Atmos. Sci.,* **44,** 542–561.

Schecter, D. A., and D. H. E. Dubin, 1999: Vortex motion driven by a background vorticity gradient. *Phys. Rev. Lett.,* **83,** 2191–2194.
——, and ——, 2001: Theory and simulations of vortex motion driven by a background vorticity gradient. *Phys. Fluids,* **13,** 1704–1723.
——, ——, A. C. Cass, C. F. Driscoll, I. M. Lansky, and T. M. O'Neil, 2000: Inviscid damping of asymmetries on a two-dimensional vortex. *Phys. Fluids,* **12,** 2397–2412.
Shapiro, L. J., and M. T. Montgomery, 1993: A three-dimensional balance theory for rapidly rotating vortices. *J. Atmos. Sci.,* **50,** 3322–3335.
Spencer, R. L., and S. N. Rasband, 1997: Damped diocotron quasi-modes of nonneutral plasmas and inviscid fluids. *Phys. Plasmas,* **4,** 53–60.
Sutyrin, G. G., 1989: Azimuthal waves and symmetrization of an intense vortex. *Sov. Phys. Dokl.,* **34,** 104–106.
——, J. C. McWilliams, and R. Saravanan, 1998: Co-rotating stationary states and vertical alignment of geostrophic vortices with thin cores. *J. Fluid Mech.,* **357,** 321–349.
Timofeev, A. V., 1992: Resonance effects in oscillations of nonuniform flows of continuous media. *Reviews of Plasma Physics,* Vol. 17, B. B. Kadomstev, Ed., Consultants Bureau, 193–301.
Viera, F., 1995: On the alignment and axisymmetrization of a vertically titled geostrophic vortex. *J. Fluid Mech.,* **289,** 29–50.
Willoughby, H. E., 1990: Temporal changes of the primary circulation in tropical cyclones. *J. Atmos. Sci.,* **47,** 242–263.